




# Light-responsive microRNA miR-211 targets Ezrin to modulate lysosomal biogenesis and retinal cell clearance

Federica Naso<sup>1,†</sup>, Daniela Intartaglia<sup>1,†</sup>, Danila Falanga<sup>1</sup>, Chiara Soldati<sup>1</sup>, Elena Polishchuk<sup>1</sup>, Giuliana Giamundo<sup>1</sup>, Paola Tiberi<sup>1</sup>, Elena Marrocco<sup>1</sup>, Paolo Scudieri<sup>1</sup>, Chiara Di Malta<sup>1</sup>, Ivana Trapani<sup>1</sup>, Edoardo Nusco<sup>1</sup>, Francesco Giuseppe Salierno<sup>1</sup>, Enrico Maria Surace<sup>1,2</sup>, Luis JV Galiotta<sup>1,2</sup>, Sandro Banfi<sup>1,3</sup> , Alberto Auricchio<sup>1,2</sup>, Andrea Ballabio<sup>1,2,4,5</sup> , Diego Luis Medina<sup>1</sup> & Ivan Conte<sup>1,6,\*</sup> 

## Abstract

Vertebrate vision relies on the daily phagocytosis and lysosomal degradation of photoreceptor outer segments (POS) within the retinal pigment epithelium (RPE). However, how these events are controlled by light is largely unknown. Here, we show that the light-responsive miR-211 controls lysosomal biogenesis at the beginning of light–dark transitions in the RPE by targeting Ezrin, a cytoskeleton-associated protein essential for the regulation of calcium homeostasis. miR-211-mediated down-regulation of Ezrin leads to Ca<sup>2+</sup> influx resulting in the activation of calcineurin, which in turn activates TFEB, the master regulator of lysosomal biogenesis. Light-mediated induction of lysosomal biogenesis and function is impaired in the RPE from miR-211<sup>-/-</sup> mice that show severely compromised vision. Pharmacological restoration of lysosomal biogenesis through Ezrin inhibition rescued the miR-211<sup>-/-</sup> phenotype, pointing to a new therapeutic target to counteract retinal degeneration associated with lysosomal dysfunction.

**Keywords** autophagy; Ezrin; miR-211; RPE; TFEB

**Subject Categories** Membranes & Trafficking; RNA Biology

**DOI** 10.15252/emboj.2019102468 | Received 13 May 2019 | Revised 3 February 2020 | Accepted 5 February 2020 | Published online 10 March 2020

**The EMBO Journal (2020) 39: e102468**

## Introduction

The retinal pigment epithelium (RPE) is a monolayer of polarized pigmented epithelial cells that resides between vessels of the choriocapillaris and the light-sensitive outer segments of photoreceptors

(PR). The RPE exerts a number of different functions for the maintenance of retinal homeostasis under stress conditions and the preservation of vision (Strauss, 1995). It provides part of the retinal–blood barrier, thus mediating selective transport of nutrients, O<sub>2</sub> and ions (Rizzolo, 2014) to the retina, and also supplies the enzymes required for isomerization of all-*trans* retinal to 11-*cis* retinal, the visual chromophore required for PR excitability (Strauss, 2005). Most importantly, the RPE prevents photo-oxidative product toxicity by contributing to the daily renewal of the PR outer segment (POS), a critical process for the maintenance of PR structural integrity and function (Nandrot *et al*, 2008; Davidson *et al*, 2011). PR continuously renew their POS via the diurnal shedding of distal spent POS tips, which are phagocytized by the RPE to rapidly clear them from the retina.

Phagocytosis of POS was recently argued to be an important trigger of autophagy in the RPE. A subset of autophagy-related proteins, including Beclin1 and ATG5, are engaged cyclically in the RPE to act in LC3-associated phagocytosis, a non-canonical form of autophagy (Kim *et al*, 2013). Once lipidated, LC3II is recruited to the POS-ingested phagosomes, which then fuse with the lysosomes forming phagolysosomes for the degradation and recycling of the ingested POS cargo (Yao *et al*, 2016). However, this process does not require the autophagy initiation complex containing Ulk1/Atg13/Fip200 proteins. These findings support a direct convergence of phagosome maturation and lysosomes for the final degradation of PR outer segments in the RPE. However, the time course of lipidated LC3II formation is delayed when compared to the peak of POS shedding and LC3-associated phagocytosis in the RPE, strongly arguing for an additional role of the lysosomal–autophagy pathway in post-phagocytosis processing of POS and re-establishment of RPE homeostasis. In addition, an oscillation of lysosomal and autophagic related genes

1 Telethon Institute of Genetics and Medicine, Pozzuoli (Naples), Italy

2 Department of Translational Medicine, University of Naples Federico II, Naples, Italy

3 Medical Genetics, Department of Biochemistry, Biophysics and General Pathology, University of Campania “L. Vanvitelli”, Naples, Italy

4 Jan and Dan Duncan Neurological Research Institute, Texas Children Hospital, Houston, TX, USA

5 Department of Molecular and Human Genetics, Baylor College of Medicine, Houston, TX, USA

6 Department of Biology, University of Naples Federico II, Naples, Italy

\*Corresponding author. Tel: +39 081 19230610; E-mail: conte@tigem.it

<sup>†</sup>These authors contributed equally to this work

was observed to be rapidly responsive to changes in light environment supporting a light-dependent regulation of lysosomal biogenesis and function other than circadian-mediated POS shedding and phagocytosis. Moreover, diurnal autophagy in the RPE ensures proficiency to deal with intracellular insults that occur from damaged mitochondria (Yao *et al*, 2014). Importantly, diurnal cargo degradation of both phagosomes and autophagosomes is critically sensitive to lysosomal biogenesis and variations in the normal levels of lysosomal proteins appear to result in a variety of retinal diseases (Frost *et al*, 2014; Ferrington *et al*, 2016; Tan *et al*, 2016; Anderson *et al*, 2017). In addition, defects in lysosomal function in the RPE have been considered to be key drivers of disease leading to conditions such as Stargardt's disease (Tan *et al*, 2016; Anderson *et al*, 2017) and age-related macular degeneration (AMD) (Wang *et al*, 2009; Ferrington *et al*, 2016), the most common cause of blindness worldwide. RPE/retina cells with diminished degradative processes are highly sensitive to the accumulation of toxic debris that can be deleterious for a large set of retinal cell lifespan in human eye diseases (Frost *et al*, 2014; Sethna *et al*, 2016; Sinha *et al*, 2016). Although each disorder results from mutations in different genes, they all share a common biochemical characteristic: abnormal accumulation of substances resulting in lysosomal dysfunction. To date, the biological mechanisms at the basis of the lysosomal biogenesis and function in RPE/PR homeostasis and disease have not been fully elucidated, nor have an effective therapy been developed to counteract retinal disorders associated with lysosomal dysfunction.

Recent discoveries have revealed that microRNAs (miRNAs), a class of small non-coding RNAs modulating mRNA translation or stability (He & Hannon, 2004), often play a key role in cellular processes acting as on/off switches. A number of these, including miR-211, are RPE/retina-associated miRNAs and show reversible, rapid up- and down-regulation during light–dark transitions (Krol *et al*, 2010). However, the functional significance of their light-dependent expression pattern in the RPE/retina remains largely unknown. Our previous work showed that miR-211 plays a key role in cone PR function and survival through the control of RPE/PR cell metabolism (Barbato *et al*, 2017). However, the link between the miR-211 molecular network and cellular metabolism and its specific influence on explicit target genes responsible for the ocular phenotype is still undefined. Here, we fill this gap by identifying Ezrin as a miR-211 target gene relevant for diurnal lysosomal biogenesis in the RPE.

We present evidence that inhibition of Ezrin induces Ca<sup>2+</sup> influx resulting in the activation of calcineurin, which in turn dephosphorylates and promotes nuclear translocation of the transcription factor EB (TFEB), the master transcriptional regulator of lysosome biogenesis and function (Settembre *et al*, 2011; Medina *et al*, 2015). This pathway is likely to play a physiologically relevant role in the RPE since mice lacking miR-211 show impaired lysosomal biogenesis and an age-dependent accumulation of phagolysosomes containing poorly processed POS, accompanied by compromised vision. Finally, we show that pharmacological inhibition of Ezrin leads to therapeutic rescue of retinal degeneration in miR-211 knockout (–/–) mice (Barbato *et al*, 2017). Thus, the identification of the mechanisms controlling lysosomal biogenesis in the RPE might be exploited for new therapeutic possibilities for the treatment of retinal degeneration associated with lysosomal dysfunction.

## Results

### miR-211 contributes to lysosomal gene expression in RPE/PR crosstalk

Control of miR-211 expression in the mouse retina is functionally linked to different light levels (Krol *et al*, 2010). This expression pattern suggested that miR-211 might modulate cellular responses to different levels of illumination, but if and how the diurnal light-dependent activation of miR-211 is necessary to maintain the homeostasis of retinal cells is still largely undefined, particularly during periods that demand high levels of lysosomal biogenesis and function. We recently demonstrated that depletion of miR-211 in homozygous mutant mice induced a progressive and specific cone dystrophy associated with an impairment of RPE/PR cell metabolism. To further explore the phenotypic consequences of miR-211 deletion and a possible link with its responsiveness to light conditions in the retina (Krol *et al*, 2010), we tested whether miR-211 is required for diurnal lysosomal biogenesis and degradative function in autophagy pathways. First, we determined whether variations in the expression levels of miR-211 and lysosomal markers in the RPE are similarly regulated by changes in the light–dark environment. MiR-211 expression levels rapidly increased in response to light in the RPE ( $\geq 30$  min after light on; Appendix Fig S1A), reaching a high expression level at 10:00 AM (3 h after light on), which coincided with diurnal lysosomal biogenesis in the RPE/retina (Appendix Fig S1A–C). Interestingly, miR-211 levels rapidly decayed following transfer of mice to the dark ( $\geq 30$  min after light off), reaching its minimum after approximately 3 h after light off [DARK (Appendix Fig S1A–C)], consistent with the previously reported data obtained for the retina (Krol *et al*, 2010). Similar kinetic data were obtained when lysosomal markers were analyzed using qRT-PCR and immunofluorescence assays ( $\geq 60$  min after light on; Appendix Fig S1A and B), supporting a molecular link between the miR-211 expression pattern and lysosomal biogenesis. Indeed, aberrant expression kinetics of lysosomal markers was detected in response to dark/light and light/dark transitions in the RPE from 2-month-old miR-211<sup>–/–</sup> compared to control mice (Appendix Fig S2A and B). These changes culminated with a significant reduction of the lysosomal marker Lamp1 in both the retina and RPE at 10:00 AM [3 h after light on (Fig 1A and B)], accompanied by a reduction of both total LC3 expression and its conversion from LC3I to the lipidated form LC3II (Fig 1B). Consistent with these results, we found a reduction of lysosomal markers (i.e., Cln5, Trpml1, and CtsD) and an increase of the Sqstm1/p62 autophagy substrate (Fig 1B) accompanied by a reduction of Cathepsin B (CtsB) activity (Fig 1C) in the RPE from 2-month-old miR-211<sup>–/–</sup> compared to control mice, suggesting that lysosomal biogenesis and function are impaired in these cells.

### miR-211 participates to lysosomal biogenesis and function in the RPE/PR crosstalk

Defective lysosomal biogenesis and degradative capacity result in the progressive accumulation of lysosomal POS/cargo substrates and lipofuscin within the RPE causing irreversible cell dysfunction and development of blinding conditions (Keeling *et al*, 2018). We sought to determine whether lysosomal substrates and lipofuscin

accumulate within the RPE in miR-211<sup>-/-</sup> mice. Morphological analysis using transmission electron microscopy (TEM) showed an age-dependent accumulation of phagolysosomes containing

poorly processed POS within the RPE of miR-211<sup>-/-</sup> mice at 10:00 AM, 3 h after light on (Fig 1D). We extended our morphological analysis to later ages, focusing on 3-, 6-, 12- and

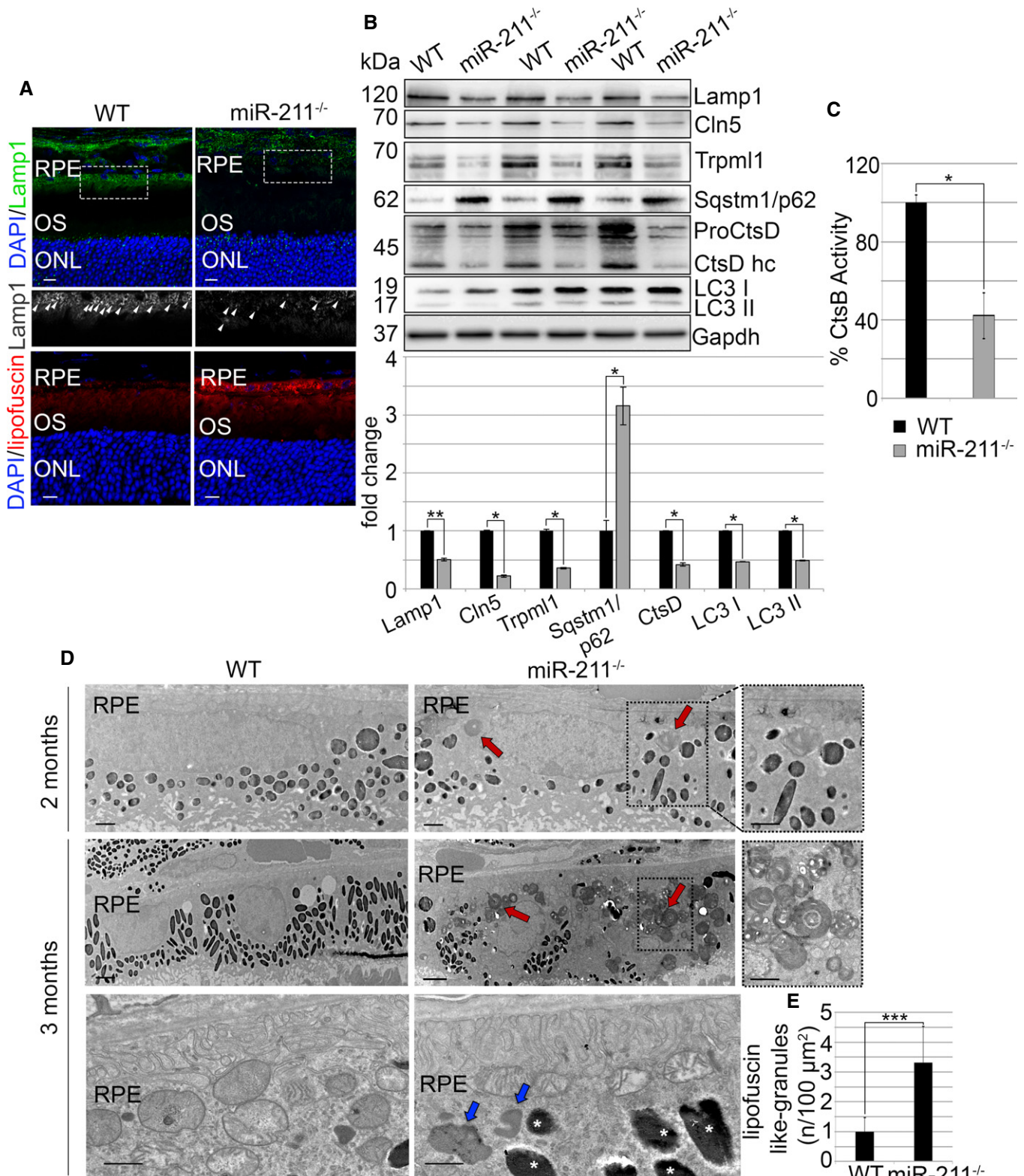


Figure 1.

**Figure 1. Phagolysosomal dysfunction in the RPE of miR-211<sup>-/-</sup> mice.**

- A Confocal images of representative eye cryosections immunostained with anti-Lamp1 antibody from 2-month-old miR-211<sup>-/-</sup> and control mice sacrificed 3 h after light on, at 10 AM (diurnal condition). Enlarged boxes highlight Lamp1-positive structures (white arrowheads) in the RPE. Autofluorescence from lipofuscin granules is visible in all cryosections of miR-211<sup>-/-</sup> compared to control littermates. Nuclei were counterstained with DAPI (blue). At least  $n = 6$  mice per group. Scale bar 10  $\mu\text{m}$ .
- B RPE was isolated at 10 AM (diurnal condition) from 2-month-old WT and miR-211<sup>-/-</sup> mice. Representative Western blot analysis of the Lamp1, Cln5, Trpm1, Sqstm1/p62, Cathepsin D (CtsD), and LC3 proteins from WT and miR-211<sup>-/-</sup> mice. Note a decrease of both pro-CtsD and its maturation CtsD heavy chain (hc). The plots show the quantification of the indicated proteins normalized to the Gapdh loading control. Bar graphs represent mean values  $\pm$  SEM of independent experiments ( $n = 6$  mice). Mann and Whitney test (miR-211<sup>-/-</sup> versus WT), \* $P \leq 0.05$ , \*\* $P \leq 0.01$ .
- C Cathepsin B (CtsB) activity in RPE lysates from 2-month-old miR-211<sup>-/-</sup> and control mice sacrificed 3 h after light on at 10 AM (diurnal condition). CtsB was reduced in miR-211<sup>-/-</sup> compared to control mice. Bar graphs represent percentage of CtsB activity  $\pm$  SEM of independent experiments ( $n = 3$  mice). Mann and Whitney test (miR-211<sup>-/-</sup> versus WT), \* $P \leq 0.05$ .
- D Representative images of conventional TEM analysis of RPE of both 2-month-old and 3-month-old WT and miR-211<sup>-/-</sup> mice. miR-211<sup>-/-</sup> mice show accumulation of phagolysosomes (red arrows) in the RPE. Scale bar 2  $\mu\text{m}$ . Enlarged boxes highlight phagolysosome-like structures containing poorly processed POS. Scale bar 1.5  $\mu\text{m}$ . Representative images of conventional TEM analysis of RPE shown at higher magnification also highlighted accumulation of lipofuscin-like granules (blue arrows) in 3-month-old miR-211<sup>-/-</sup> compared to control WT mice. Melanosomes are indicated by white asterisks. Scale bar 500 nm ( $n = 3$  mice).
- E Graphs showing number of lipofuscin-like granules ( $n/100 \mu\text{m}^2$ ) from the RPE of 3-month-old miR-211<sup>-/-</sup> mice as in (D). Bar graphs represent mean values  $\pm$  SEM. Mann and Whitney test (miR-211<sup>-/-</sup> versus WT) \*\*\* $P \leq 0.005$  ( $n = 6$  mice).

Data information: (RPE) retinal pigment epithelium; (OS) outer segment; (ONL) outer nuclear layer.  
Source data are available online for this figure.

18-month-old animals. Interestingly, we observed an age-dependent progressive increase of POS marker-positive phagolysosomes [LIGHT (at 10:00 AM, 3 h after light on)] in the RPE of miR-211<sup>-/-</sup> compared to control mice (Fig 1D and Appendix Fig S2C and D). Furthermore, the number of rhodopsin positive structures was abnormally high 3 h after light off [DARK; (10:00 PM)] in the RPE of 6-month-old miR-211<sup>-/-</sup> compared to control mice (Appendix Fig S2C and E), supporting an impairment of lysosomal cargo processing in the absence of miR-211. Consistent with this, from the age of 2 months onwards, miR-211<sup>-/-</sup> mice showed an accumulation of lipofuscin-like granules (Fig 1A, D and E). This phenotype is in accordance with previous studies that showed dysfunctional phagocytic/autophagy-lysosomal pathways in AMD (Wang *et al*, 2009; Ferrington *et al*, 2016) and Stargardt's disease (Anderson *et al*, 2017), both characterized by lipofuscin accumulation and impairment of PR cone function and survival, reinforcing the relevance of miR-211 function in RPE cell clearance. To further corroborate this notion, 3-month-old GFP-LC3 transgenic mice, stably expressing the autophagosome membrane marker LC3 fused with GFP (GFP-LC3) (Mizushima *et al*, 2004; Settembre *et al*, 2011), were subretinally injected with an adeno-associated virus (AAV) vector encoding the human miR-211 precursor (AAV 2/8-miR-211) or with scramble. We found that compared to scramble there was an increase in diurnal lysosomal biogenesis 1 month after injection (Fig EV1A–E). Notably, both retina and RPE specimens from miR-211-injected animals showed a significant increase in the number of autophagosomal GFP:LC3-positive and endo/lysosomal Lamp1-positive vesicles (Lamp1 positive spots, hereafter referred as lysosomes; Fig EV1A, C and D) as well as their co-localization (LC3-Lamp1-positive spots—Fig EV1A and E). Western blot analysis also confirmed a significant increase in both Lamp1 and lipidated LC3II protein levels (at 10:00 AM, 3 h after light on) accompanied by a decrease of the Sqstm1/p62 autophagy substrate (Fig EV1F) in AAV 2/8-miR-211-injected RPE cells compared to controls. Altogether, these data strongly support that miR-211 stimulates diurnal lysosomal biogenesis in RPE/PR crosstalk.

**miR-211 controls lysosomal biogenesis by targeting Ezrin**

To provide insights into how miR-211 regulates lysosomal biogenesis, we searched for relevant miR-211 target genes exhibiting an anti-correlative expression pattern with respect to miR-211 in our previously generated *in vivo* and *in vitro* RNA-seq datasets (Conte *et al*, 2014, 2015; Barbato *et al*, 2017). The *Ezrin* gene, a member of the ERM (Ezrin/Radixin/Moesin) family of membrane-cytoskeleton linkers, appeared particularly attractive to explain the observed RPE/PR defects since it has been shown previously to be strongly expressed in the RPE (Bonilha *et al*, 1999) and highly sensitive to light exposure (Zhang *et al*, 2017). Consistent with our transcriptome analysis, it was recently described and validated as a miR-211 target gene (Zhang *et al*, 2018) and, more importantly, its upregulation resulted in a decrease of lysosomal Lamp1 expression levels (Federici *et al*, 2009; Bian & Murad, 2014). A combination of these features was not observed for any previously validated miR-211 target (Chou *et al*, 2018), none of which appears to be related to lysosomal biogenesis (Table EV1). Based on these observations, we investigated the expression pattern of *Ezrin* and found an anti-correlation with that of miR-211 (Fig 2A and B). It rapidly decreased in response to light in the RPE ( $\geq 30$  min after light on), reaching a low expression level at 10:00 AM (3 h after light on). Conversely, its expression rapidly increased in response to dark conditions in the RPE ( $\geq 30$  min after light off), showing high expression 3 h after light off in the RPE of wild-type (WT) mice (Fig 2A and B). We found that there were increased Ezrin transcript and protein levels in the RPE of miR-211<sup>-/-</sup> mice compared to control littermates at 10:00 AM (3 h after light on), when physiologically it should be poorly expressed (Fig 2C–E). Notably, we observed that the kinetics of *Ezrin* gene expression in response to dark/light and light/dark transitions were absent in the RPE from miR-211<sup>-/-</sup> mice (Fig 2F). As a control, the kinetics of the expression of miR-211's host gene (*Trpm1*) was not altered in the RPE from miR-211<sup>-/-</sup> when compared with control animals (Fig 2G). Consistent with this, qRT-PCR analysis confirmed the proper expression levels of genes adjacent to *Trpm1* (*Mtmr10* and *Klf13*; Fig 2H), in line with our previous

results (Barbato *et al*, 2017). These observations further indicate the specificity of miR-211 depletion and support the notion that impairment of lysosomal biogenesis upon light stimulation is a consequence of the lack of miR-211-mediated repression of *Ezrin*. Accordingly, miR-211 overexpression *in vivo* caused the opposite behavior resulting in a significant reduction of Ezrin levels accompanied by an increase in lysosomal biogenesis. In particular, we found that subretinal administration of AAV 2/8-miR-211 resulted in a decrease in endogenous Ezrin mRNA and protein levels in the RPE/PR of the injected GFP-LC3 transgenic mice, as detected by immunofluorescence, Western blot, and qRT-PCR analyses (Fig EV1A, F and G).

### miR-211 controls autophagic flux *in vitro*

We next sought to determine whether the miR-211<sup>-/-</sup> phenotype was indeed related to abnormal activation of *Ezrin* expression. In order to minimize the variability due to interference of high cell confluence on the analysis of lysosomal biogenesis and autophagy as previously reported (Fuentes *et al*, 2003), we employed a “sub-confluence” strategy (i.e., 80% cell confluence) for all *in vitro* experiments. We found that genetic silencing of miR-211 (anti-miR-211) in the ARPE-19 cell line markedly reduced the number of structures with the ultrastructural characteristics of lysosomes, and where lysosome-like structures could be identified, they stained poorly for LAMP1 as demonstrated by immuno-electron microscopy (IEM) (Fig EV2A–D). As expected, we found that silencing of miR-211 led to an increase in EZRIN expression levels (Fig EV2E–G and Appendix Fig S3A). Western blot and immunofluorescence analyses also confirmed the reduced expression of lysosomal markers LAMP1, LC3, TRPML1, CLN5, and CTSD (Fig EV2E and Appendix Fig S3A), a decrease in the number of LC3/LAMP1-positive vesicles (Appendix Fig S3A and B) and an increase of SQSTM1/

p62 (Fig EV2E) compared to control cells (anti-miR-ctrl), consistent with previous results described in the RPE from miR-211<sup>-/-</sup> mice. Furthermore, silencing of miR-211 induced a block of the autophagic flux as determined by LC3II lipidation in starved (stv) cells in the presence of bafilomycin (baf) (Appendix Fig S3C). By contrast, miR-211 overexpression (miR-211) *in vitro* induced a significant increase in the number of structures with the ultrastructural characteristics of lysosomes, which appeared highly labeled with LAMP1 as demonstrated by IEM (Fig EV2A–D). In addition, miR-211 overexpression caused a decrease in EZRIN expression levels (Fig EV2E–G and Appendix Fig S3A) accompanied by an increase in the expression of the lysosomal markers and a reduction in the SQSTM1/p62 autophagy substrate (Fig EV2E and Appendix Fig S3A) compared with control cells (miR-ctrl). To further corroborate the latter result, we also analyzed the effect of miR-211 overexpression on the autophagic flux. Interestingly, we found that, in response to miR-211 overexpression, the increased lysosomal biogenesis was accompanied by an increase in autophagosome–lysosome fusion as demonstrated by the increased number of LC3/LAMP1-positive vesicles (Appendix Fig S3A and B), and an induction of the autophagic flux as determined by LC3II lipidation in starved (stv) cells in the presence of bafilomycin (baf) (Appendix Fig S3D). Taken together, these data suggest that miR-211-mediated targeting of Ezrin is an important regulator of lysosomal biogenesis and autophagy pathways in RPE.

### Ezrin inhibition promotes lysosomal biogenesis and function *in vitro*

To further corroborate the possible interplay between miR-211 activity and Ezrin inhibition as well as their contribution to lysosomal biogenesis, we tested the impact of Ezrin function on both lysosomal biogenesis and function using pharmacologically and

**Figure 2. miR-211 controls Ezrin expression *in vivo*.**

- A Representative confocal images of eye cryosections immunostained with anti-Ezrin (green) and anti-ZO-1 (red) antibodies from 2-month-old WT mice sacrificed 3 h after light on at 10 AM (diurnal condition—LIGHT) and 3 h after light off at 10 PM (nocturnal condition—DARK), nuclei were counterstained with DAPI (blue). Enlarged boxes highlight Ezrin staining in both basal infoldings (BI) and apical extension (AE) of the RPE. At least  $n = 6$  mice per group. Scale bar 10  $\mu\text{m}$ .
- B Graph representing the kinetic expression pattern of *Ezrin* levels in the RPE from 2-month-old WT mice during dark/light and light/dark transitions. Mice were sacrificed at determined time points as indicated on the x-axis. Scheme at the top describes light/dark adaptation regime. Values normalized to *Hprt* represent means  $\pm$  SEM. Mann and Whitney test  $^*P \leq 0.05$  ( $n = 3$  mice for each time point). Values from 12-h dark-adapted mice (T0) were set to one.
- C Confocal images of representative eye cryosections immunostained with anti-Ezrin (green) and anti-ZO-1 (red) antibodies from 2-month-old miR-211<sup>-/-</sup> and WT control mice sacrificed 3 h after light on at 10 AM (diurnal condition). Enlarged boxes highlight Ezrin staining in both basal infoldings (BI) and apical extension (AE) of the RPE. At least  $n = 6$  mice per group. Scale bar 10  $\mu\text{m}$ .
- D qRT-PCR assay for *Ezrin* from RPE 2-month-old WT and miR-211<sup>-/-</sup> mice sacrificed 3 h after light on at 10 AM. The graph shows the expression level of *Ezrin* normalized to *Hprt*. Bar graphs represent mean values  $\pm$  SEM. Mann and Whitney test (miR-211<sup>-/-</sup> versus WT),  $^{***}P \leq 0.005$  ( $n = 6$  mice).
- E RPE was isolated at 10 AM (diurnal condition) from 2-month-old WT and miR-211<sup>-/-</sup> mice. Representative image at low exposure of Western blot analysis of the Ezrin protein from WT and miR-211<sup>-/-</sup> mice. The graph shows the quantification of Ezrin normalized to the *Gapdh* loading control. Bar graphs represent mean values  $\pm$  SEM of independent experiments ( $n = 5$  mice). Mann and Whitney test (miR-211<sup>-/-</sup> versus WT),  $^{**}P \leq 0.01$ .
- F Graph representing the kinetic expression pattern of *Ezrin* levels in the RPE from 2-month-old miR-211<sup>-/-</sup> mice during dark/light and light/dark transitions. Mice were sacrificed at determined time points as indicated in x-axis. Scheme at the top describes light/dark adaptation regime. Values normalized to *Hprt* represent means  $\pm$  SEM ( $n = 3$  mice for each time point). Values from 12-h dark-adapted mice (T0) were set to one.
- G Graph representing the kinetic expression pattern of *Trpm1* levels in the RPE from 2-month-old WT mice during dark/light and light/dark transitions. Mice were sacrificed at determined time points as indicated in x-axis. Scheme at the top describes light/dark adaptation regime. Values normalized to *Hprt* represent means  $\pm$  SEM ( $n = 3$  mice for each time point). Values from 12-h dark-adapted mice (T0) were set to one.
- H qRT-PCR assay for *Mtmr10* and *Klf13* from RPE 2-month-old WT and miR-211<sup>-/-</sup> mice sacrificed 3 h after on at 10 AM. The graph shows the expression level of these genes normalized to the *Hprt*. Bar graphs represent mean values  $\pm$  SEM ( $n = 3$  mice).

Data information: (RPE) retinal pigment epithelium; (OS) outer segment; (ONL) outer nuclear layer; (BI) RPE basal infoldings; (AE) RPE apical extensions. Source data are available online for this figure.

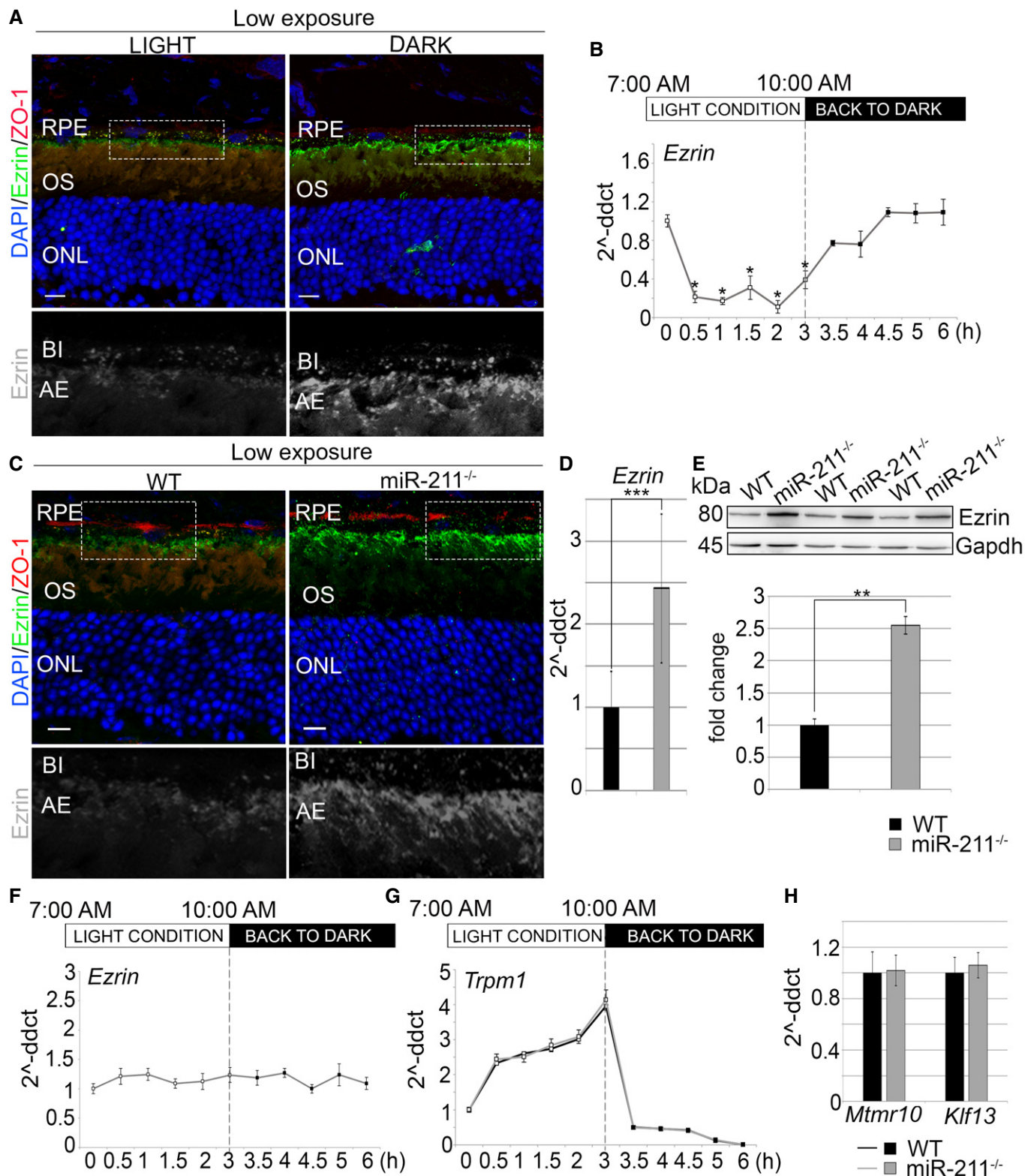


Figure 2.

genetically based inhibition approaches. Phosphorylation of Ezrin at the amino acid residue 567 (Thr567), within the COOH-terminal ERM association domain (C-ERMAD), leads to an open

conformation and enables the interaction of an active Ezrin with other proteins (Turunen *et al*, 1994; Gary & Bretscher, 1995; Matsui *et al*, 1998, 1999; Barret *et al*, 2000). Importantly, T567-Ezrin

phosphorylation has been reported to be specifically inhibited by the small molecule “NSC668394” via its binding to Ezrin without altering total Ezrin protein levels (Bulut *et al*, 2012).

Culturing ARPE-19 cells in the presence of NSC668394 led to a significant increase in the number of lysosomes and upregulated lysosomal markers, as demonstrated by immunofluorescence (Fig 3A and B), Western blot (Fig 3C), and IEM (Appendix Fig S4A and B) analyses. Western blot analysis also confirmed the activation of Cathepsin D (CTSD), as detected by increase of its mature heavy chain, and the reduction of the autophagy substrate SQSTM1/p62 in ARPE-19 cells treated with NSC668394 compared with vehicle-control cells (DMSO) (Fig 3C), supporting the notion that pharmacological inhibition of Ezrin promoted lysosomal biogenesis and function. NSC668394 treatment was also found to induce an increased rate of autophagosome–lysosome fusion as assessed by LC3 and LAMP1 co-localization (Fig 3A and B) and using an LC3 protein tandem-tagged with red fluorescent protein–green fluorescent protein (RFP-GFP) (Kimura *et al*, 2007; Settembre *et al*, 2011). Autophagosomes (GFP<sup>+</sup> and RFP<sup>+</sup>) were discriminated from autophagolysosomes (GFP<sup>-</sup> and RFP<sup>+</sup>) because of quenching of the GFP signal (but not of RFP) inside the acidic lysosomal compartment (Fig 3D and E). Consistent with this observation, starvation (stv) treatment in the presence of bafilomycin (baf) showed a further increase of LC3II in NSC668394-treated ARPE-19 cells (Appendix Fig S4C), confirming the presence of increased autophagic flux and excluding that lipidated LC3II accumulation was due to a block along the autophagy pathway. Notably, autophagic cells were not apoptotic, as indicated by their normal nuclear morphology (Fig 3). Next, we reasoned that if inhibition of Ezrin directly controls expression of lysosomal biogenesis and function, the levels of the enzymatic activity of lysosomal Cathepsin B (CTSB) should be increased and the autophagy substrates should be reduced. Therefore, we carried out a Magic red assay, based on a Cathepsin B-specific substrate that, upon hydrolysis, liberates membrane-impermeable fluorescent cresyl violet within lysosomes containing catalytically active CTSB in living cells. Indeed, we found an increase in the intensity of the Magic Red in NSC668394-treated compared with control cells (Fig 3F and G). These data were further validated biochemically by an enzymatic activity assay of CTSB (Fig 3H). Notably, similar to what we observed in NSC668394 treated cells, silencing of *Ezrin* (*siEZR*) resulted in an induction of lysosomal biogenesis and autophagic flux (Appendix Fig S4D–F and Appendix Fig S5A–E), demonstrating that both pharmacological and genetic inhibition of Ezrin phenocopy the increase of lysosomal biogenesis and function observed in miR-211 overexpressing cells.

### **Ezrin overexpression suppresses lysosomal biogenesis and function *in vitro***

To obtain additional support for the relevance of miR-211-mediated regulation of Ezrin and to demonstrate that increased Ezrin expression levels account for lysosomal dysregulation observed in miR-211 deficiency, we analyzed the effects of GFP-tagged versions of WT-Ezrin or the constitutively active mutant T567D-Ezrin (Coscoy *et al*, 2002) on lysosomal biogenesis in normally fed ARPE-19 cells. We found that both WT-Ezrin:GFP (EZRIN:GFP) and T567D-Ezrin:GFP expression resulted in repression of lysosomal biogenesis as assessed by immunofluorescence staining for LAMP1 and Western

blot analysis for autophagic markers as well as an increase in the autophagy substrate SQSTM1/p62 (Fig EV3A and B) compared to GFP control cells. Notably, we found that repression of lysosomal biogenesis in WT-Ezrin:GFP, but not in NSC668394-unresponsive T567D-Ezrin:GFP, overexpressing cells was rescued by NSC668394 treatment (Fig EV3A and B). Taken together, these data indicate that upregulation of Ezrin suppresses lysosomal biogenesis *in vitro* and that NSC668394 specifically triggers Ezrin inhibition thorough T567-Ezrin dephosphorylation, resulting in activation of lysosomal biogenesis. We reasoned that if most of the changes in lysosomal markers caused by NSC668394 are specifically mediated by Ezrin inhibition, NSC668394 administration on Ezrin-silenced cells should not further increase lysosomal marker expression levels. This was the case since we did not observe any additional increase in lysosomal biogenesis and autophagy in Ezrin-silenced ARPE-19 cells upon NSC668394 treatment (Fig EV3C and D).

We next sought to determine whether the miR-211 phenotype was indeed related to abnormal activation of *Ezrin* expression by performing a series of rescue experiments. Pharmacological and genetic inhibition of *Ezrin* rescued lysosomal dysregulation in the miR-211 loss of function in the ARPE-19 cell line (Appendix Fig S6A–D). Collectively, these data indicate that miR-211 activity is very likely to be Ezrin dependent, because reduction of both Ezrin expression and activity rescued the anomalies in lysosomal biogenesis.

### **Inhibition of Ezrin induces Ca<sup>2+</sup>-mediated triggering of Calcineurin and modulates TFEB nuclear translocation**

Ezrin is a widely expressed protein that links the actin cytoskeleton to various proteins and has been shown to be involved in a large spectra of cellular functions (e.g., cell motility, cell–cell, and cell–matrix recognition) that depends on its conformational state and its interactors (Brambilla & Fais, 2009). Ezrin has been also reported to regulate Ca<sup>2+</sup> homeostasis in different cell types through its essential role in retaining ion channels within multiprotein complexes at the plasma membrane (Lockwich *et al*, 2001; Padanyi *et al*, 2010; Hatano *et al*, 2013). Importantly, release of lysosomal Ca<sup>2+</sup> mediated by the channel mucolipin 1 (TRPML1) modulates the protein phosphatase calcineurin (PPP3CB) (Medina *et al*, 2015), which in turn dephosphorylates and activates TFEB (Medina *et al*, 2015), a master regulator of the CLEAR (Coordinated Lysosomal Expression and Regulation) network, of lysosomal biogenesis, and of the autophagy pathway (Settembre *et al*, 2011; Settembre & Medina, 2015). We therefore hypothesized that if Ezrin directly controls lysosomal biogenesis through Ca<sup>2+</sup>/calcineurin-mediated activation of TFEB, both pharmacologically and genetically based inhibition of Ezrin should activate TFEB-mediated lysosomal biogenesis in cells.

Indeed, analysis by high-content (HC) live imaging demonstrated that both administration of the inhibitor NSC668394 or silencing of Ezrin (*siEZR*) significantly promoted nuclear translocation of both endogenous and overexpressed TFEB in normally fed HeLa (HeLa<sup>TFEB-GFP</sup>) [*siCTRL* (Fig 4A and B)] and ARPE-19 cell lines (Fig EV4A), similar to starvation (stv) that was used as a control. Accordingly, inhibition of Ezrin induced a downshift of TFEB protein in fed cells (Fig 4E), confirming its dephosphorylation as assessed by Western blot analysis. Most remarkably, siRNA-mediated inhibition of calcineurin (*siPPP3CB*) in Ezrin-inhibited

cells abolished the nuclear translocation of TFEB (Fig 4A, C and D), suggesting that inhibition of Ezrin might trigger  $Ca^{2+}$  influx inducing the activation of calcineurin, which in turn promotes

dephosphorylation and TFEB nuclear translocation. Therefore, we hypothesized that the link between Ezrin and lysosomal biogenesis might involve TRPML1-dependent  $Ca^{2+}$  release. To test this

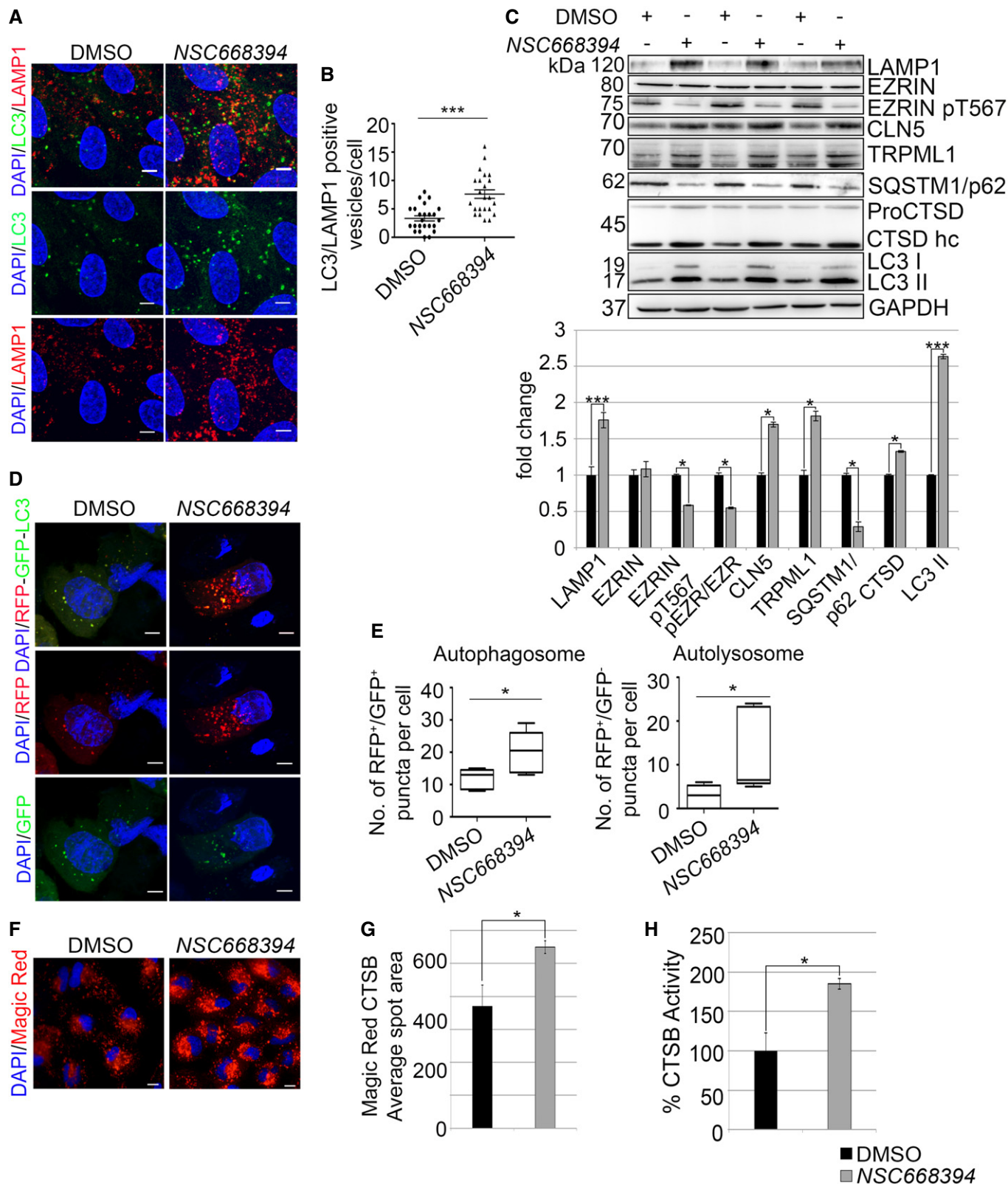


Figure 3.



**Figure 3. Pharmacological inhibition of Ezrin results in autophagy induction in ARPE-19 cells.**

- A Representative images from ARPE-19 cells treated with DMSO and NSC668394. All cells were fixed and stained with anti-LC3 (green) and anti-LAMP1 (red) antibodies and nuclei were counterstained with DAPI (blue). Scale bar 5  $\mu$ m.
- B The plot shows the quantification of the numbers of LC3/LAMP1-positive vesicles per cell ( $n \geq 100$ ). Values represent means  $\pm$  SEM from three independent experiments. Student's *t*-test (NSC668394 versus DMSO) \*\*\* $P \leq 0.005$ .
- C Representative Western blots of LAMP1, EZRIN, EZRIN-pT567, CLN5, TRPML1, SQSTM1/p62, CTSD, and LC3 proteins from DMSO or NSC668394 treated cells. Note an increase of both pro-CTSD and its maturation CTSD heavy chain (hc). The plot shows the quantification of the indicated proteins normalized to the GAPDH loading control. Bar graphs represent mean values  $\pm$  SEM of at least  $n = 6$  independent experiments. Mann and Whitney test (NSC668394 versus DMSO) \* $P \leq 0.05$ , \*\*\* $P \leq 0.005$ .
- D Representative images of RFP-GFP-LC3 assay in ARPE-19 cells transiently transfected with RFP-GFP-LC3 and treated with DMSO or NSC668394. Nuclei were counterstained with DAPI (blue). Scale bars: 5  $\mu$ m.
- E Box plots showing quantitative analysis of RFP<sup>+</sup>GFP<sup>+</sup> puncta (Autophagosome) and RFP<sup>+</sup>GFP<sup>-</sup> puncta (autolysosome) ( $n \geq 100$  cells) from three independent experiments. Box limits represent 25<sup>th</sup> percentile and 75<sup>th</sup> percentile; horizontal lines represent medians; whiskers display min. to max. values. Student's *t*-test (NSC668394 versus DMSO) \* $P \leq 0.05$ .
- F Endolysosomal Cathepsin activity was revealed by incubation with Cathepsin B (CTSB) Magic Red substrate for 20 min and images of the living cell collected on the HC analysis. Scale bar 10  $\mu$ m.
- G Graph showing the mean values of intensity of cresyl violet fluorescence  $\pm$  SEM of representative data ( $n \geq 100$  cells) from three independent experiments. Mann and Whitney test (NSC668394 versus DMSO) \* $P \leq 0.05$ .
- H Cathepsin B (CTSB) activity in lysates from NSC668394-treated and DMSO-control ARPE-19 cells. Graph showing the percentage of values  $\pm$  SEM of CTSB activity from 4 independent experiments. Mann and Whitney test (NSC668394 versus DMSO) \* $P \leq 0.05$ .

Source data are available online for this figure.

hypothesis, we monitored calcium dynamics in the close proximity of lysosomal membranes using the fluorescent calcium-sensitive GCaMP3 probe fused to TRPML1 (Medina *et al*, 2015). We triggered TRPML1 activity with the selective activator ML-SA1. Addition of this compound resulted in a rapid localized calcium increase that showed a fast decline to near resting levels in approximately 100 s (Fig 4F). Notably, cells receiving NSC668394, or genetically silenced for *Ezrin*, showed a much more sustained response to ML-SA1 (Fig 4F and Appendix Fig S5F). Furthermore, this sustained phase was highly sensitive to ML-SI3, a specific inhibitor of TRPML1 (Fig 4F). Therefore, our results indicate that Ezrin inhibition results in a potentiation of TRPML1 sensitivity to activating stimuli. Consistent with these findings, we also found that treatment with the specific Ca<sup>2+</sup> chelator BAPTA-AM significantly reduced TFEB nuclear translocation in Ezrin-inhibited cells, further supporting that Ca<sup>2+</sup>-dependent calcineurin activation acts downstream of Ezrin (Fig 4G and H). Altogether these data demonstrate that inhibition of Ezrin induces TFEB nuclear translocation by promoting Ca<sup>2+</sup>-mediated triggering of calcineurin, thus revealing a previously unidentified role for Ezrin in this cellular process.

### The TFEB-mediated CLEAR network is regulated by Ezrin

To obtain additional support for the relevance of Ezrin-mediated regulation of TFEB nuclear translocation, we carried out a series of *in vitro* and *in vivo* experiments. The ability of Ezrin to modulate TFEB-mediated lysosomal biogenesis and autophagy was further confirmed by the upregulation of TFEB target CLEAR gene expression after Ezrin inhibition (Fig 4I) and the absence of alterations in CLEAR gene expression after Ezrin inhibition in HeLa<sup>TFEB-KO</sup> cells (Fig EV4B and C). Moreover, this Ezrin activity is very likely to be TFEB-dependent, because Ezrin overexpression (EZRIN:GFP) in HeLa<sup>TFEB-KO</sup> cells did not alter the expression of autophagic markers (Fig EV4D). We next sought to determine whether the Ezrin-induced phenotype was indeed related to a possible defective TFEB nuclear translocation. Previous studies have shown that starvation conditions result in lysosomal Ca<sup>2+</sup> release via TRPML1 and consequently TFEB nuclear translocation (Medina *et al*, 2015). We

reasoned that if Ezrin modulates Ca<sup>2+</sup> flux, the levels of TFEB nuclear translocation under starvation conditions should be reduced in the Ezrin-overexpressing cells because of alterations in Ca<sup>2+</sup> flux. Indeed, analysis by HC live imaging demonstrated that overexpression of an mCherry-tagged version of Ezrin (EZRIN-mCherry) significantly impaired nuclear translocation of TFEB in a starved HeLa<sup>TFEB-GFP</sup> cell line (Fig EV4E and F). We next sought to determine whether the miR-211 retinal phenotype was indeed related to Ezrin-mediated impairment of TFEB activity by performing an *in vivo* rescue experiment. To this end, we used an AAV 2/8:CMV-hTFEB<sup>S142A-S211A</sup>:3XFLAG construct (AAV hTFEB) that encoded a constitutively nuclear active form of TFEB (Young *et al*, 2016). We injected AAV hTFEB subretinally in one eye and AAV 2/8-CMV-EGFP (eGFP) as a control in the contralateral eye of miR-211<sup>-/-</sup> mice. The animals were sacrificed 15 days after the injection to avoid the possibility that high expression of TFEB might induce tumors (Giatromanolaki *et al*, 2015) and to allow maximal, sustained expression of the vector. Notably, following AAV hTFEB delivery, a significant rescue of the lysosomal Lamp1 expression accompanied by an increase of the lipidated form of LC3II (Fig EV4G–I) was detected in the transduced retinal area of the TFEB-injected eye in comparison with the contralateral GFP-injected eye of miR-211<sup>-/-</sup> mice at 10:00 AM (3 h after light on). These data support the existence of a previously unidentified molecular network in the RPE by which miR-211 directly controls lysosomal biogenesis through the repression of Ezrin-mediated control of Ca<sup>2+</sup>-induced triggering of calcineurin and TFEB nuclear translocation.

### Pharmacological inhibition of Ezrin rescues miR-211<sup>-/-</sup> phenotypes

Impairment of the endocytic/autophagy–lysosomal pathways has been frequently implicated in the AMD phenotype that is associated with lipofuscin accumulation, lysosomal dysfunction and severe cone defects reflected in macular atrophy and central vision loss (Ferrington *et al*, 2016; Keeling *et al*, 2018). Interestingly, the dysfunction of lysosomal biogenesis and function observed in

miR-211<sup>-/-</sup> mice was accompanied by both lipofuscin accumulation in the RPE and by cone dystrophy (Barbato *et al*, 2017). Previous studies have shown that induction of lysosomal function results in

an enhancement of POS degradation and a decrease of lipofuscin accumulation (Guha *et al*, 2012; Zhang *et al*, 2015). Therefore, if most of the phenotypic consequences caused by miR-211 depletion

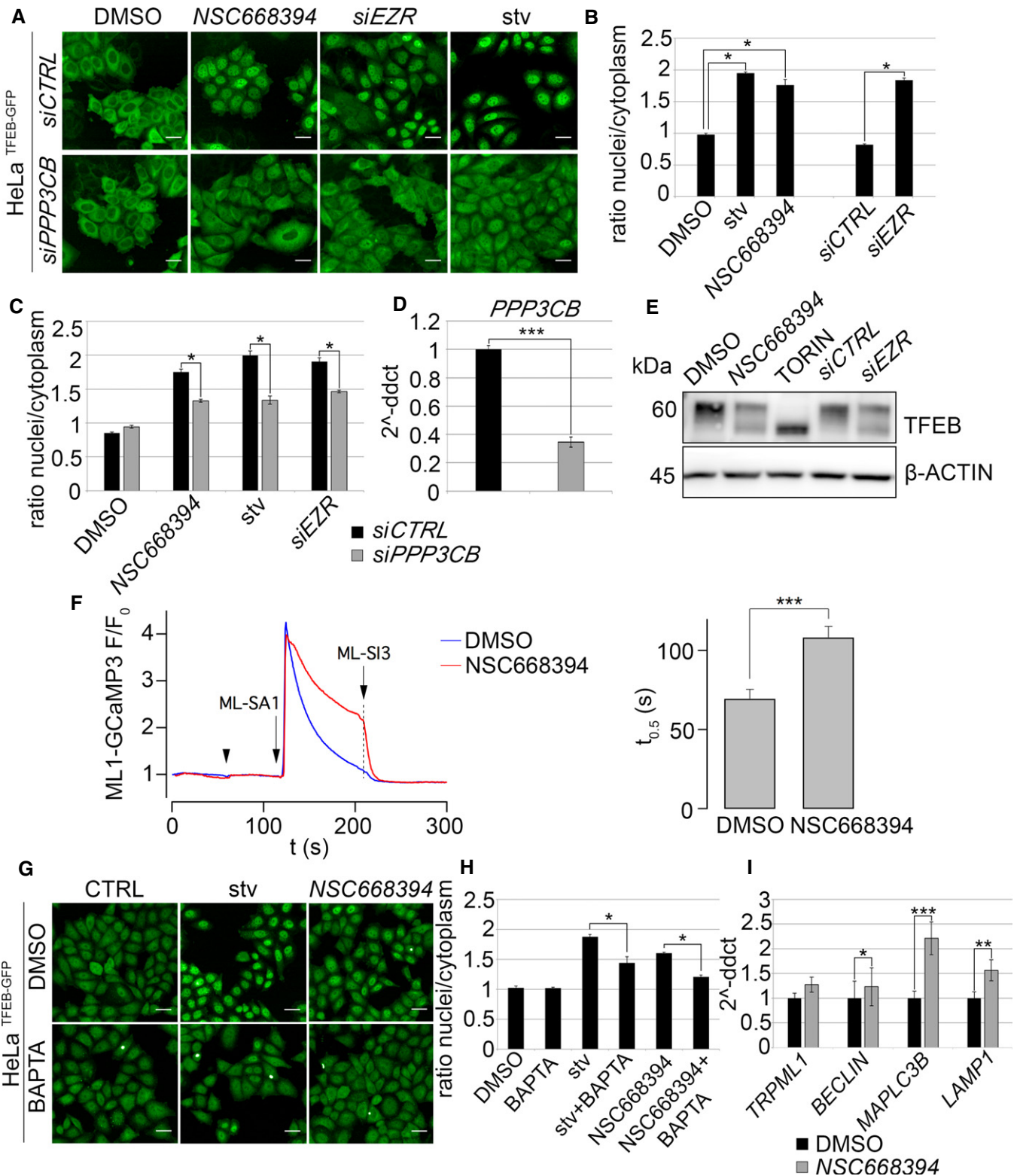


Figure 4.

**Figure 4. Ezrin inhibition results in TFEB nuclear translocation.**

- A Representative images from HC assay of HeLa<sup>TFEB-GFP</sup> cells transfected with control (siCTRL) or siPPP3CB and subjected to the indicated conditions. Analysis of TFEB nuclear translocation in HeLa<sup>TFEB-GFP</sup> cells transfected with siCTRL or siPPP3CB and treated with DMSO or NSC668394, silenced for EZRIN (siEZR), or serum-starved (stv). Both pharmacological inhibition and silencing of Ezrin induced TFEB nuclear localization in stable HeLa<sup>TFEB-GFP</sup> cells. Starvation (stv) was used as control. Nuclear translocation of TFEB in stable HeLa<sup>TFEB-GFP</sup> cells subjected to the indicated conditions is rescue after silencing of PPP3CB. Scale bar 5  $\mu$ m.
- B The graph shows the mean  $\pm$  SEM of the percentage of nuclear TFEB translocation in Ezrin-inhibited cells compared to control;  $n = 3$  independent experiments were performed. Mann and Whitney test (NSC668394 and stv versus DMSO; siEZR versus siCTRL)  $*P \leq 0.05$ .
- C The graph shows the mean  $\pm$  SEM of the percentage of nuclear TFEB translocation in Ezrin-inhibited cells and subjected to the silencing of PPP3CB. At least three independent experiments were performed. Mann and Whitney test (siPPP3CB versus siCTRL)  $*P \leq 0.05$ .
- D qRT-PCR assay for PPP3CB from HeLa<sup>TFEB-GFP</sup> cells transfected with siPPP3CB and siCTRL. The graph shows the reduction in PPP3CB expression level normalized to the Hprt. Bar graphs represent mean values  $\pm$  SEM Mann and Whitney test (siPPP3CB versus siCTRL),  $***P \leq 0.005$  ( $n = 6$  independent experiments).
- E Both pharmacological inhibition and silencing of EZRIN induce downshift of endogenous TFEB electrophoretic mobility in Western blot analysis. Torin treatment was used as control.
- F Representative traces of ML1-GCaMP3 normalized fluorescence recorded in transiently transfected ARPE-19 cells. During time-lapse recording, cells were stimulated with ML-SA1 (20  $\mu$ M) after addition (arrowhead) of DMSO or NSC668394. Where indicated, the specific ML1 inhibitor ML-S13 (10  $\mu$ M) was added. Bar graph reports the mean values  $\pm$  SEM of the time required by fluorescence to decay to half of the ML-SA1-induced peak.  $n = 50$  cells from three independent experiments.  $***P < 0.005$  by Mann and Whitney test.
- G Nuclear translocation of TFEB in stable HeLa<sup>TFEB-GFP</sup> cells subjected to the indicated conditions is reduced after Ca<sup>2+</sup> chelator BAPTA treatment. Scale bar 5  $\mu$ m.
- H The graph shows the mean  $\pm$  SEM of the percentage of nuclear TFEB translocation in Ezrin-inhibited cells compared with DMSO under Ca<sup>2+</sup> chelator BAPTA treatment. At least three independent experiments were performed. Mann and Whitney test (stv, stv+BAPTA, BAPTA, NSC668394, NSC668394+BAPTA versus DMSO)  $*P \leq 0.05$ .
- I qRT-PCR analysis for TFEB target genes (*TRPML1*, *BECLIN1*, *MAPLC3B*, and *LAMP1*) was performed on ARPE-19 cells treated with DMSO or NSC668394. Bar graphs represent mean values  $\pm$  SEM of at least three independent experiments. Mann and Whitney  $*P \leq 0.05$ ,  $**P \leq 0.01$ ,  $***P \leq 0.005$ .

Source data are available online for this figure.

*in vivo* are due to Ezrin-mediated impairment of diurnal lysosomal biogenesis and function, a daily drug-mediated pulsatile induction of autophagy by a temporal inhibition of Ezrin should re-establish normal expression levels of lysosomal markers and rescue both RPE and retinal phenotype. To validate this hypothesis and to dissect the potential of therapeutic induction of lysosomal biogenesis in the RPE/retina crosstalk, we inhibited Ezrin function for 2 h by a daily intraperitoneal injection of NSC668394, at a dose of 0.226 mg/kg, whose pharmacokinetic studies have largely demonstrated a monophasic elimination after 2 h from the plasma (Celik *et al*, 2016). Daily injection of NSC668394 over two consecutive weeks was efficient in inducing lysosomal biogenesis and function in the RPE/retina of 3-month-old GFP-LC3 transgenic mice. Both retina and RPE specimens from injected animals showed a significant increase in the number of Lamp1-positive and GFP-LC3/Lamp1-positive vesicles as well as a significant increase in both the lysosomal marker Lamp1 and lipidated LC3II levels (2 h after injection) when compared with vehicle-injected (DMSO) control animals (Fig EV5A and B). We next asked whether an NSC668394-mediated increase in the expression of lysosomal genes/proteins might improve “handling” of autophagolysosomes in the RPE. We reasoned that if NSC668394 directly controls lysosomal function *in vivo*, the degradation kinetics of the autophagy substrate Sqstm1/p62 should be increased in the RPE from animals treated with a single acute administration of lysosomal inhibitor chloroquine upon NSC668394 treatment. As expected, Western blot analysis showed a faster decrease of Sqstm1/p62 in the RPE from NSC668394-treated animals compared to vehicle-treated animals (DMSO) (Fig EV5C).

Consistent with these observations, daily injections of NSC668394 to miR-211<sup>-/-</sup> mice over five consecutive months (beginning at 1 month old of age), but not vehicle, restored the active pT567-Ezrin to normal expression levels, but not total Ezrin protein levels (Fig 5A), and in turn normalized the diurnal lysosomal biogenesis and activity in the RPE/retina of miR-211<sup>-/-</sup> mice, as demonstrated by recovery of both the lysosomal marker Lamp1 and

lipidated LC3II levels and reduction in the autophagy substrate Sqstm1/p62 in diurnal conditions (Fig 5A and B).

These changes were associated with a rescue of Cathepsin B (CtsB) activity (Fig 5C), accompanied by a similar trend in the enzymatic activity of  $\beta$ -glucuronidase (GUSB), albeit the latter was not statistically significant (Fig 5D). Consistent with these findings, we observed a rescue of accumulation of both phagosomes and double-membrane phagolysosomes containing poorly processed POS within the RPE of miR-211<sup>-/-</sup> mice as detected by TEM analysis (Fig 6A). Moreover, a significant decrease in rhodopsin accumulation within the RPE was found by immunostaining with an anti-Rhodopsin antibody (Fig 6B), further supporting a rescue of phagolysosomal cargo processing. Notably, from the age of 3 months onwards, NSC668394-treated miR-211<sup>-/-</sup> mice showed a decrease of lipofuscin (Fig 6B and C). Most importantly, we measured a significant recovery of cone number and density defects in NSC668394-treated miR-211<sup>-/-</sup> mice at 3 and 6 months of age compared to control miR-211<sup>-/-</sup> mice (miR-211<sup>-/-</sup> + DMSO) (Fig 6B and D, Appendix Fig S7A and B), as demonstrated by quantifying cones that were labeled by immunostaining with anti-cone-Arrestin antibody. As a consequence, we observed a progressive rescue in retinal function by both standard electroretinographic (ERG) and 6-Hz scotopic flicker ERG recordings (Alfano *et al*, 2011) in NSC668394-treated miR-211<sup>-/-</sup> mice compared to control mice. We found that both rod and cone responses in NSC668394-treated miR-211<sup>-/-</sup> mice were similar to those recorded in WT mice (Fig 6E and F, Appendix Fig S7C–F).

Altogether, our data unmask a molecular network in daily cell clearance in the RPE/PR crosstalk that requires the miR-211-mediated activation of both lysosomal biogenesis and function through repression of Ezrin. Moreover, our findings reveal a previously unidentified role for Ezrin in this cellular process and identify a new drug that might be exploited for new therapeutic possibilities for the treatment of retinal degeneration associated with lysosomal dysfunction.

## Discussion

It is well established that two independent autophagy pathways support diurnal waste clearance in the RPE and both are finely regulated by circadian and non-circadian processes, with a daily induction that relies on and occurs after the peak period of POS disk-shedding and can be evoked by a light pulse (Kim *et al*, 2013; Muniz-Feliciano *et al*, 2017). Although our understanding of the regulation of autophagy pathways has improved, a gap remains in our understanding on how the diurnal activation of both lysosomal biogenesis and function is generated, maintained, and successively repressed daily upon a switch from dark to light conditions in the RPE. MiR-211 has discrete and dynamic expression domains in the

RPE/retina, its expression being highly controlled by light–dark conditions (Krol *et al*, 2010). *In vitro* studies have shown that miR-211 contributes to RPE differentiation and homeostasis (Wang *et al*, 2010; Dai *et al*, 2015). To date, however, miR-211 function in the RPE has not been thoroughly analyzed and its *in vivo* role in this tissue remains unclear. Interestingly, recent findings suggest that induction of miR-211 expression correlates with an increase in autophagosomes during osteogenic differentiation (Ozeki *et al*, 2017) and with repression of the mTOR pathway during cellular stress (Ozturk *et al*, 2019), but the mechanism of action in these processes was largely unknown.

The results described herein indicate that miR-211-mediated repression of Ezrin is necessary for both daily-inducing

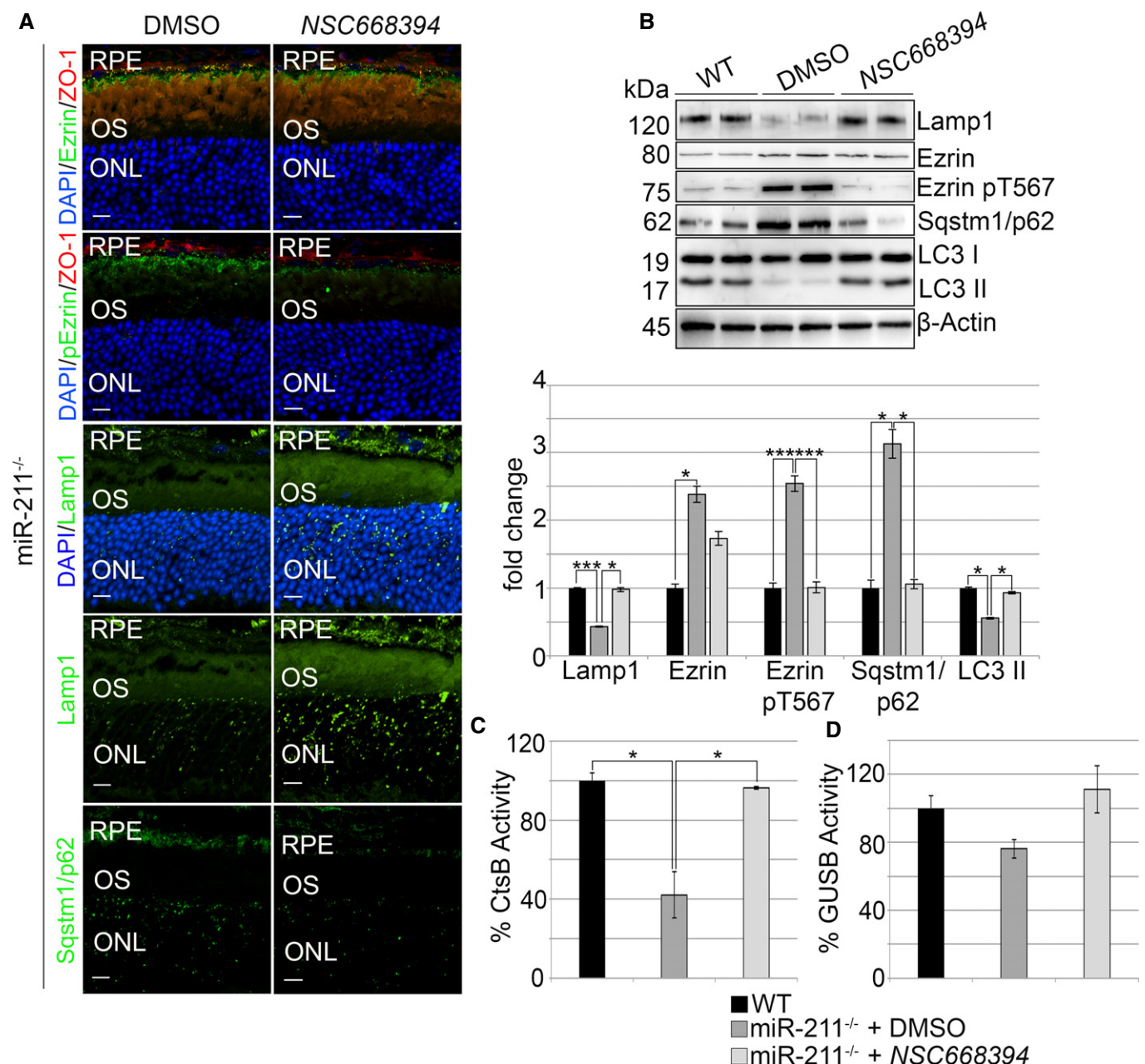


Figure 5.

**Figure 5. NSC668394 rescues lysosomal biogenesis in miR-211<sup>-/-</sup> mice.**

- A Confocal images of representative eye cryosections immunostained with anti-Ezrin (green)/anti-ZO-1 (red), anti-Ezrin-pT567 (green)/anti-ZO-1 (red), anti-Lamp1 (green), and anti-Sqstm1/p62 (green) antibodies from 6-month-old miR-211<sup>-/-</sup> sacrificed 5 months after DMSO or NSC668394 treatment. Nuclei are counterstained with DAPI (blue). At least  $n = 6$  mice per group. Scale bar 100  $\mu\text{m}$ .
- B RPE was isolated 5 months after DMSO or NSC668394 treatment from 6-month-old miR-211<sup>-/-</sup> mice. Representative Western blot proteins from these tissues were performed to determine the expression levels of Lamp1, Ezrin, Ezrin-pT567, Sqstm1/p62, and LC3. The plots show the quantification of the indicated proteins normalized to the  $\beta$ -actin loading control. Bar graphs represent mean values  $\pm$  SEM of independent experiments ( $n = 6$  mice). Mann and Whitney test (DMSO versus WT; NSC668394 versus DMSO), \* $P \leq 0.05$ , \*\*\* $P \leq 0.005$ .
- C Cathepsin B (CtsB) activity in RPE lysates from miR-211<sup>-/-</sup> and WT mice sacrificed 3 h after light on at 10 AM (diurnal condition). RPE was isolated 1 week after DMSO or NSC668394 treatment from 2-month-old miR-211<sup>-/-</sup> mice. CtsB was rescued in NSC668394-treated miR-211<sup>-/-</sup> compared to DMSO-control miR-211<sup>-/-</sup> mice. Bar graphs represent percentage of CtsB activity  $\pm$  SEM of independent experiments ( $n = 3$  mice). Mann and Whitney test (DMSO-miR-211<sup>-/-</sup> versus WT; NSC668394-miR-211<sup>-/-</sup> versus DMSO-miR-211<sup>-/-</sup>), \* $P \leq 0.05$ .
- D GUSB activity from retina from miR-211<sup>-/-</sup> and control mice sacrificed 3 h after light on at 10 AM (diurnal condition). Retina was isolated 1 week after DMSO or NSC668394 treatment from 2-month-old miR-211<sup>-/-</sup> mice. GUSB was rescued in NSC668394-treated miR-211<sup>-/-</sup> compared to DMSO-control miR-211<sup>-/-</sup> mice. Bar graphs represent percentage of GUSB activity  $\pm$  SEM of independent experiments ( $n = 3$  mice). Mann and Whitney test (DMSO-miR-211<sup>-/-</sup> versus WT; NSC668394-miR-211<sup>-/-</sup> versus DMSO-miR-211<sup>-/-</sup>).

Data information: (RPE) retinal pigment epithelium; (OS) outer segment; (ONL) outer nuclear layer. Source data are available online for this figure.

phagolysosomal and autophagolysosomal cargo degradation in the RPE. We found that this lysosome-regulating pathway is mediated by an increase in TRPML1-dependent  $\text{Ca}^{2+}$ , which, as a second messenger, triggers activation of calcineurin and stimulation of lysosomal biogenesis and waste clearance via the TFEB-mediated transcriptional network. This regulatory cascade is strongly supported by a number of observations. In the RPE, a daily switch from dark to light conditions induces miR-211 expression (Krol *et al*, 2010), which in turn targets and represses Ezrin. The inhibition of Ezrin promotes a  $\text{Ca}^{2+}$ -mediated activation of calcineurin, which in turn leads to an increase in both TFEB dephosphorylation and TFEB nuclear translocation thus inducing the expression of lysosomal and autophagic genes (Fig 7). Conversely, during dark conditions, miR-211 is down-regulated leading to upregulation of Ezrin which is activated by phosphorylation on threonine Thr567 at the carboxyl-terminal C-ERMAD domain, which in turn represses  $\text{Ca}^{2+}$ -mediated activation of calcineurin. An imbalance in this molecular network during the switch from dark to light conditions in miR-211<sup>-/-</sup> mice

induces a diurnal impairment of lysosomal biogenesis with consequent defective phagolysosomal and autophagolysosomal cargo processing. These dysfunctions cause age-dependent lipofuscin accumulation and possibly cone degeneration. This last possibility is highly likely, because cones are more sensitive to lipofuscin accumulation and stress (Conley *et al*, 2012). In support of this interpretation, a daily pulsatile drug-mediated inhibition of Ezrin function was sufficient to restore the levels of active Ezrin form to values statistically indistinguishable from those of the control eyes, rescuing lysosomal pathways, lipofuscin accumulation and most importantly the miR-211<sup>-/-</sup> ocular phenotype.

Interestingly, previous studies implicated distinct and context-dependent targeting activities for miR-211 and its paralog miR-204 depending on the cellular environment (Abraham *et al*, 2016; Vitiello *et al*, 2017). In cancer, miR-204 upregulation was shown to inhibit autophagic flux by targeting both LC3 and Caveolin1-mediated repression of  $\text{Ca}^{2+}$  flux (Xiao *et al*, 2011; Hall *et al*, 2014). More recently, miR-204 deletion in the RPE was associated with

**Figure 6. Pharmacological inhibition of Ezrin rescues the miR-211<sup>-/-</sup> phenotype.**

- A Representative images of conventional TEM analysis of RPE of WT, DMSO-treated miR-211<sup>-/-</sup> mice, and NSC668394-treated miR-211<sup>-/-</sup> 3-month-old mice. NSC668394-treated miR-211<sup>-/-</sup> mice show rescue of accumulation of double-membrane phagolysosome-like structures containing poorly processed POS (red arrows) compared to DMSO-treated miR-211<sup>-/-</sup> mice. Scale bar 1  $\mu\text{m}$ .
- B Confocal images of representative eye cryosections immunostained with anti-Rhodopsin (green) antibody from WT and miR-211<sup>-/-</sup> mice at 3 months of age after DMSO or NSC668394 treatment, which are sacrificed 3 h after light on at 10 AM (diurnal condition). Nuclei are counterstained with DAPI (blue). At least  $n = 6$  mice per group. Scale bar 100  $\mu\text{m}$ . The enlarged box highlights rhodopsin accumulation in the RPE (green spots). Scale bar 5  $\mu\text{m}$ . Autofluorescence from lipofuscin granules from WT and miR-211<sup>-/-</sup> mice at 3 months of age after DMSO or NSC668394 treatment. Representative images of retina cryosections immunostained with anti-Cone-Arrestin (green) antibody from WT and miR-211<sup>-/-</sup> mice at 3 months of age after DMSO or NSC668394 treatment. Nuclei are counterstained with DAPI (blue).  $N =$  at least 6 mice per group. Scale bar 100  $\mu\text{m}$ .
- C Graphs showing number of lipofuscin granules from the RPE of mice as in (B). Bar graphs represent mean values  $\pm$  SEM. Mann and Whitney test (miR-211<sup>-/-</sup> DMSO versus WT and miR-211<sup>-/-</sup> NSC668394 versus DMSO-treated mice) \*\*\* $P \leq 0.005$ . \* $P \leq 0.05$  ( $n = 6$  mice).
- D Graphs show cone percentage (cones/area) from the retina of mice treated as in (B). Error bars represent SEM. Mann and Whitney test (DMSO versus WT and NSC668394 versus DMSO-treated mice) \*\*\* $P \leq 0.005$  ( $n = 6$  mice).
- E Representative flicker traces at 3 months of age show the rescue of flicker responses of NSC668394-treated miR-211<sup>-/-</sup> mice (green lines) compared to DMSO-treated miR-211<sup>-/-</sup> control mice (red lines). WT mice were used as a control (black lines). Flicker recordings were performed with light intensities ranging from 10–4 to 15  $\text{cd s/m}^2$  in steps of 0.6 logarithmic units at 6 Hz frequency.
- F Flicker responses, plotted as a function of stimulus intensity, from WT (black lines), DMSO-treated miR-211<sup>-/-</sup> (red lines), and NSC668394-treated miR-211<sup>-/-</sup> (green lines) mice, at 3 months of age. The amplitude of the recordings from NSC668394 miR-211<sup>-/-</sup> treated mice is significantly rescued compared to DMSO-treated miR-211<sup>-/-</sup> mice. WT mice were used as a control. Error bars represent SEM. ANOVA test (DMSO versus WT and NSC668394 versus DMSO-treated mice) \*\* $P \leq 0.01$ , \*\*\* $P \leq 0.005$ .

Data information: (OS) outer segment; (ONL) outer nuclear layer; (RPE) retinal pigment epithelium.

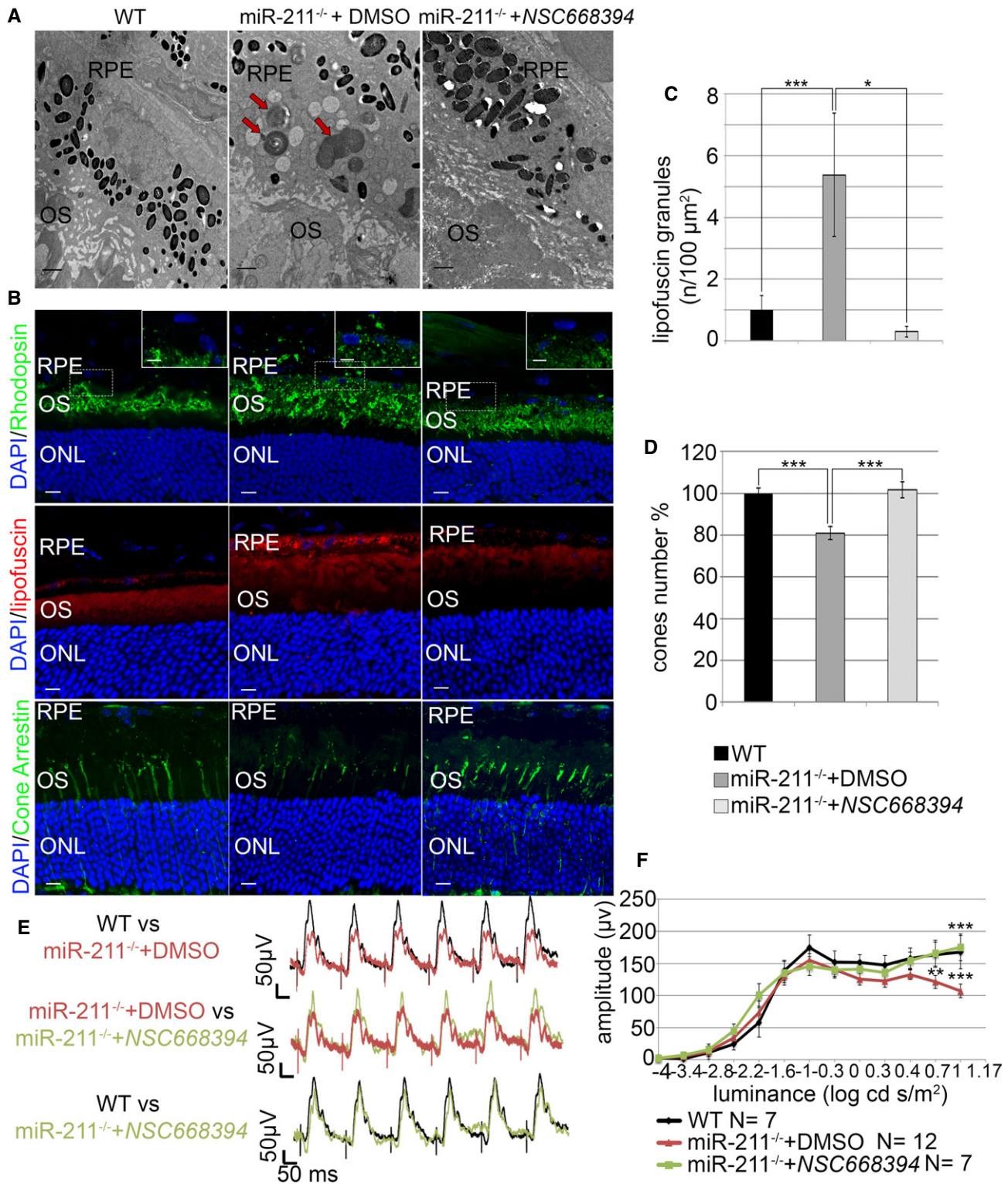
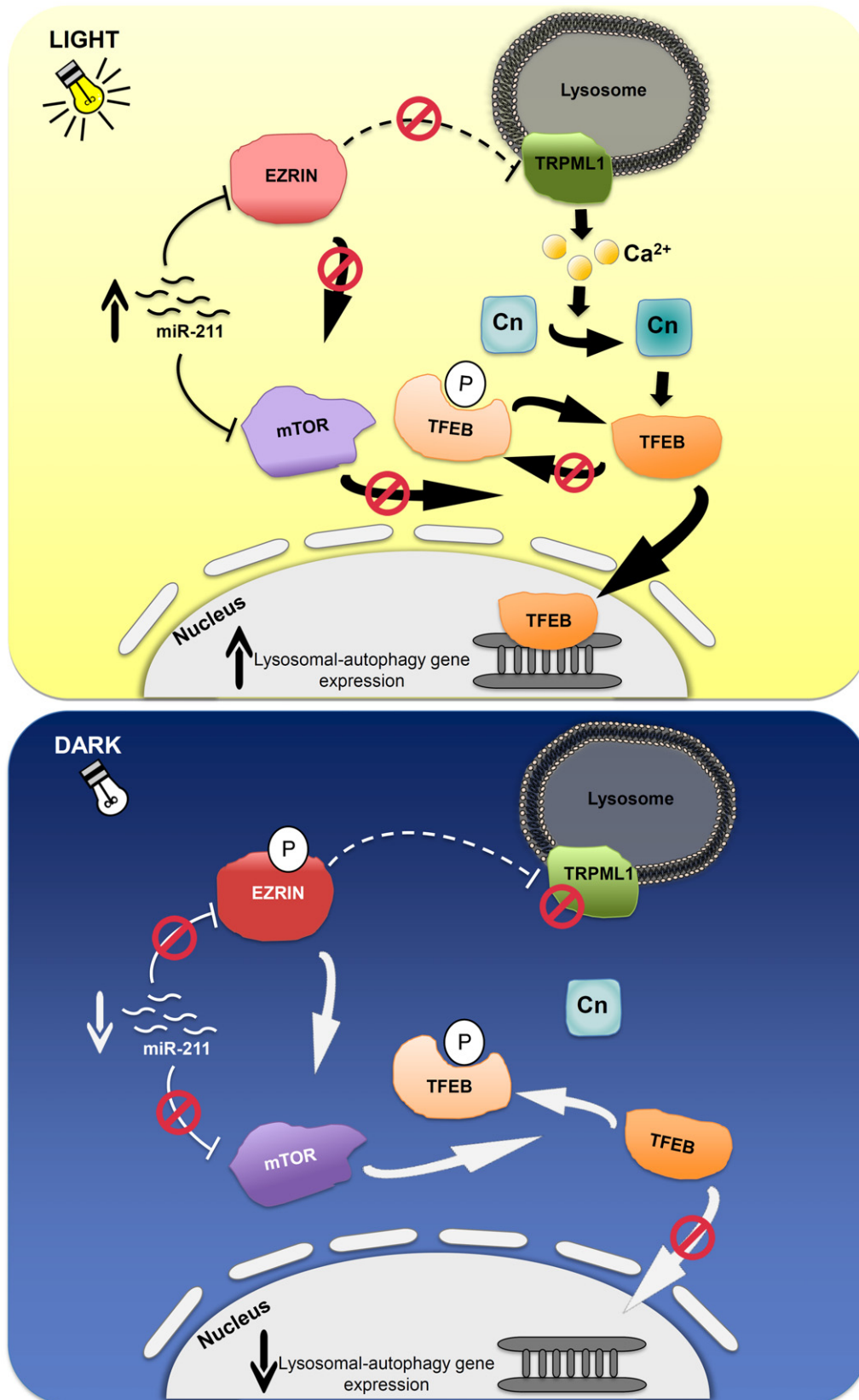


Figure 6.

strong upregulation of autophagic markers accompanied by an imbalance of phagocytic degradation (Zhang *et al.*, 2019), in line with previous results (Muniz-Feliciano *et al.*, 2017). Notably, miR-

204 and its host gene, namely TRPM3, show an expression pattern opposite to that of miR-211 in the retinal ONL (Krol *et al.*, 2010). These observations together with our data highlight the complexity



**Figure 7. Model of miR-211-mediated regulation of lysosomal biogenesis and function.**

Under light-phase conditions, Ezrin is repressed by miR-211. The inhibition of Ezrin releases a Ca<sup>2+</sup> microdomain flux into cells through the TRPML1 channel. This leads to calcineurin (Cn) activation and lysosomal biogenesis via TFEB nuclear translocation. Under night-phase conditions, miR-211 is down-regulated, this in turn induces Ezrin upregulation and repression of TFEB-mediated lysosomal biogenesis. Both miR-211 and Ezrin may converge on and integrate into the mTOR pathway.

of the function of miRNAs operating in the RPE to control cell clearance, suggesting that these two miRNAs could be antagonistic and be key elements in modulating the light-dependent lysosomal/autophagic pathways.

Of note, the ocular phenotype in the miR-211<sup>-/-</sup> mice resembles that observed in animal models of human pathological conditions such as Stargardt's disease and AMD. The use of miR-211 in gene therapy is also being explored to promote RPE and PR survival in AMD (Cunnusamy *et al*, 2012). Therefore, it is of the utmost importance to identify all miR-211's functions and targets to determine whether alterations in miR-211 expression and its targets may contribute to the pathogenesis of AMD in humans.

Several targets of miR-211 have been identified in cancer cells. However, whether and how miR-211 target genes might modulate lysosomal biogenesis in cells is largely unexplored. Recent findings identified Ezrin as the most promising candidate target gene participating in the miR-211 ocular phenotype: First, Ezrin is highly expressed in the RPE; second, its expression is opposite to miR-211 and modulated by light stimulus; and third, upregulation of Ezrin has been proposed to reduce Lamp1 expression. Our findings help to define the relevance of the miR-211/Ezrin axis in lysosomal biogenesis in the RPE upon light stimulus. They also provide mechanistic insights into how the Ca<sup>2+</sup>-dependent calcineurin network originates from the miR-211-mediated inhibition of Ezrin, an important regulatory protein that links cell membrane proteins to actin (Fehon *et al*, 2010).

Previous studies reported that the NH2-terminal FERM domain of Ezrin has a dominant negative effect on Ezrin function (Crepaldi *et al*, 1997; Zhao *et al*, 2004). Recent findings have reported that the FERM domain of Ezrin induces both the assembly of the actin scaffold at the phagosome membrane and phagolysosomal fusion (Marion *et al*, 2011). Interestingly, the composition of the phagosome membrane, its degradative contents, and the phosphorylated status of the C-terminus of the Ezrin protein appear to be crucial components for the actin assembly machinery to facilitate phagolysosomal fusion (Erwig *et al*, 2006). Notably, the amino acid sequence of Ezrin contains unique phosphorylation sites (Y353, Y477, and T567) in the C-terminal C-ERMAD domain, suggesting that Ezrin may have multiple context-dependent roles depending on its phosphorylation state. Y353-phosphorylated Ezrin was shown to regulate the JNK activation pathway in endosomes (Parameswaran *et al*, 2013), whereas Y477 phosphorylation of Ezrin regulates growth and invasion of Src-transformed epithelial cells (Heiska *et al*, 2011). Moreover, Ezrin overexpression was found to mediate invasion via the AKT/mTOR signal transduction pathway (Krishnan *et al*, 2006) and Ezrin inhibition was found to inhibit the mTOR pathway (Wan *et al*, 2005), a major signaling pathway controlling lysosomal function.

Intriguingly, Lamp1 on late endosomes was found to be a key factor for the phosphorylation of Ezrin at amino acid residue 567 (Thr567) on the C-ERMAD domain (Parameswaran *et al*, 2013; Bian & Murad, 2014). However, an increase in Ezrin expression resulted in a reduction of Lamp1 in cancer cells (Federici *et al*, 2009) and affected Lamp1 protein levels in RPE cells (Bian & Murad, 2014). We envisage that Ezrin recruitment and phosphorylation of residue Thr567 on the C-ERMAD domain might play distinct roles in lysosomal biogenesis, phagolysosome, and autophago-lysosome fusion at distinct stages of lysosomal-mediated waste clearance in the RPE. In

support of this hypothesis, the simultaneous observations of lysosome-opposite diurnal recruitment of Ezrin and its phosphorylated Thr567-active form in dark conditions and the following dismissal and dephosphorylation in light condition demonstrate the need for a strict spatial and temporal restriction of Ezrin function in the RPE. Our findings further suggest that Ezrin-exerted inhibition of the lysosomal pathway is very likely to be Ca<sup>2+</sup>-dependent and mediated by regulation of calcineurin and its target TFEB. Importantly, Ezrin has been reported to participate in retaining Ca<sup>2+</sup> ion channels within multiprotein complexes at cytoplasmic membranes and to regulate Ca<sup>2+</sup> homeostasis in different cell types (Lockwich *et al*, 2001; Padanyi *et al*, 2010; Hatano *et al*, 2013). Here, we found a yet unreported function of Ezrin inhibition in inducing an increased rate of Ca<sup>2+</sup>-mediated activation of calcineurin through potentiation of TRPML1 sensitivity and the corresponding activation of lysosomal biogenesis and autophagy via TFEB nuclear translocation. Thus, miR-211/Ezrin axis might ensure correct lysosomal biogenesis by also controlling TRPML1 phosphorylation status. This last possibility is particularly attractive, because phosphorylation of the C-terminal TRPML1 serine residues regulates its autophagic function (Onyenwoke *et al*, 2015). However, the mode of induction of lysosomal biogenesis and function by miR-211-mediated Ezrin inhibition may be more complex than our initially envisaged by also involving a direct regulation of the mTOR pathway (Fig 7).

Importantly, the potential applications of our newly identified molecular network extend beyond the comprehensive and highly relevant identification of diurnal regulation of endocytic/autophagy-lysosomal pathways in the RPE/retina crosstalk. Recently, several attempts have been made to develop therapeutic pharmacological approaches to treat AMD in which lipofuscin has accumulated. However, despite initial promising results, developing therapeutic strategies to treat AMD still represents a challenge. Our study shows the efficacy of induction of lysosomal biogenesis and activity, via pharmacological repression of Ezrin, for the clearance of lipofuscin accumulation in the miR-211<sup>-/-</sup> mice, which could represent an important therapeutic strategy to treat lysosomal impairment associated with retinal diseases including the most common cause of blindness worldwide such as age-related macular degeneration (Wang *et al*, 2009; Ferrington *et al*, 2016).

## Materials and Methods

### Animals

The miR-211 knockout mouse line (mir-211<sup>-/-</sup>) employed in this study was generated by the Wellcome Trust Sanger Institute as previously described (Barbato *et al*, 2017). For the ISH experiments, CD1 albino mice were used as previously described (Karali *et al*, 2010). All studies on animals were conducted in strict accordance with the institutional guidelines for animal research and approved by the Italian Ministry of Health; Department of Public Health, Animal Health, Nutrition and Food Safety in accordance with the law on animal experimentation (article 7; D.L. 116/92; protocol number: 00001/11/IGB; approval date June 6, 2011). Furthermore, all animal treatments were reviewed and approved in advance by the Ethics Committee of Ospedale Cardarelli (Naples, Italy). MiR-211<sup>-/-</sup> mice were maintained on the C57Bl/6J background. In all



experiments, we used as controls aged-matched littermates of miR-211<sup>-/-</sup> mice.

### Subretinal injection of AAV vectors in mice

GFP-LC3 mice were housed at the Institute of Genetics and Biophysics animal house (Naples, Italy) and maintained under a 12-h light/dark cycle (10–50 lux exposure during the light phase). Mice were anesthetized as previously described (Gargiulo *et al*, 2012); then, AAV 2/8 vectors were delivered subretinally via a trans-scleral trans-choroidal approach as described by Liang *et al* (2001). All eyes were treated with 1  $\mu$ l of AAV 2/8 vector solution, at a dose of  $1 \times 10^9$  genome copies/eye. Mice were sacrificed 1 month post-injection as previously described (Barbato *et al*, 2017). Overnight dark adaptation of mice was performed before sacrifice. This study was carried out in accordance with the Association for Research in Vision and Ophthalmology Statement for the Use of Animals in Ophthalmic and Vision Research and with the Italian Ministry of Health regulation for animal procedures. All procedures were submitted to the Italian Ministry of Health; Department of Public Health, Animal Health, Nutrition and Food Safety. Surgery was performed under anesthesia and all efforts were made to minimize suffering.

### Drug treatments and Light/Dark adaptation of mice for tissue isolation

Drug treatments were performed by once-daily intraperitoneal injection of NSC668394, at a dose of 0.226 mg/kg, as previously described (Celik *et al*, 2016). For chloroquine assays, animals underwent to single intraperitoneal injection of 100 mg/kg chloroquine as previously described (Gaynes *et al*, 2008) followed by NSC668394 administration. Light/dark adaptation of treated mice was performed following standard procedures (Krol *et al*, 2010). In particular, the mice were maintained in dark condition with maximum of 0.4 lux from 19:00 pm to 7:00 am. Then, animals were kept in a room with the light phase (450 lux) from 7:00 am to 19:00 pm. For light/dark transition studies, some animals were transferred after 3 h from light condition to dark condition and sacrificed to selected time points. Tissues from DA mice were isolated under dim red light.

### Electrophysiological recordings

Scotopic and photopic electrophysiological recordings were performed as described (Barbato *et al*, 2017). A National Instruments amplifier with a xenon Ganzfeld stimulator (CSO, Costruzione Strumenti Oftalmici, Florence, Italy) was used to record miR-211 mice. Briefly, mice were dark-adapted for 3 h. Animals were anesthetized and positioned in a stereotaxic apparatus under dim red light. Their pupils were dilated with a drop of 0.5% tropicamide (Visufarma, Rome, Italy), and body temperature was maintained at 37.5°C. The electrophysiological signals were recorded through gold-plate electrodes inserted under the lower eyelids in contact with the cornea. The electrodes in each eye were referred to a needle electrode inserted subcutaneously at the level of the corresponding frontal region. The different electrodes were connected to a two-channel amplifier. For ERG analysis in dark-adapted

conditions (scotopic), eyes were stimulated with light flashes. Eleven different light intensity stimuli were used ranging from  $1 \times 10^{-4}$  to 20 cd s/m<sup>2</sup>. Amplitudes of a- and b-waves were plotted as a function of increasing light intensity. After completion of responses obtained in scotopic conditions, the recording session continued with the purpose of dissecting the cone pathway through the photopic ERG. Photopic cone responses were isolated in light conditions with a constant background illumination of 50 cd/m<sup>2</sup>, with 10 flashes and a light intensity of 20 cd s/m<sup>2</sup>. Cone response was then better isolated using Flicker analysis (An *et al*, 2012). Mice were stimulated with a fixed frequency of 6 Hz and flashes of 13 different light intensities, ranging from  $10^{-4}$  to 15 cd s/m<sup>2</sup> generated by the Ganzfeld stimulator. To minimize the noise, different responses evoked by light were averaged for each luminance step.

### Western blot analysis

Mouse eyes were enucleated and the RPE was separated from the retina. Cells were collected after transfections or treatments to extract total protein. Both mice and cell samples were lysed by using RIPA buffer (150 mM sodium chloride, 1% Triton X-100, 0.5% sodium deoxycholate, 0.1% sodium dodecyl sulfate, 50 mM Tris, pH 8.0) with inhibitors cocktail (Thermo Fischer Scientific, 78420). The concentration of total protein was determined by Bradford analysis and quantified by using a NanoDrop ND-8000 spectrophotometer (NanoDrop Technologies). Proteins were fractionated by sodium dodecyl sulfate–polyacrylamide gel electrophoresis (SDS–PAGE) and transferred to PVDF membranes (EMD Millipore, IPVH00010), then blocked in Tween 0.1%–Tris-buffered saline containing 5% non-fat milk or 5% bovine serum albumin (Sigma-Aldrich, 9048-46-8) for 1 h at room temperature and subsequently incubated overnight at 4°C with primary antibodies. For Western blot analysis, the following antibodies were used: mouse anti-Lamp1 (1:500, Sigma-Aldrich, L1418), rabbit anti-Cln5 (1:1,000, Abcam AB126306), rabbit anti-Trpml1 (1:1,000, ALOMONE Lab ACC-081), rabbit anti-LC3 (1:1,000, Novus LC3B/MAP1LC3B), rabbit anti-SQSTM1/p62 (1:1,000, Sigma-Aldrich, P0067), mouse anti-CtsD (1:1,000, Santa Cruz SC-377124), mouse anti-Ezrin (1:1,000, Novex, 357300), rabbit anti-phospho-Ezrin (Th567) that detects endogenous levels of Ezrin only when phosphorylated at threonine 567 (1:700 Sigma-Aldrich, PA5-37763), mouse anti-Gapdh (1:1,000, Santa Cruz, SC-32233), mouse anti- $\beta$ -actin (1:700, Sigma-Aldrich, A5441), anti-TFEB (1:1,000 Cell Signaling, 4240), mouse anti-FLAG (1:1,000, Sigma, F3165). After washing with 1% TBS, the membranes were incubated for 1 h at room temperature with the following secondary antibodies: goat anti-rabbit IgG antibody, HRP conjugate, and goat anti-mouse IgG antibody HRP conjugate (1:10,000 EMD Millipore, 12-348; 12-349). Western blot detection was done with a GE detector (GE Healthcare Life Sciences) and quantified using ImageJ software. To check retina contamination, the protein levels of photoreceptors (Rhodopsin) marker were analyzed as control in RPE protein samples.

### Immunofluorescence

Mouse eyes were fixed overnight in 4% paraformaldehyde in PBS at 4°C and then cryopreserved by treatment first with 15% and then

with 30% sucrose in phosphate-buffered saline and embedded in OCT. Twelve-micrometer cryosections were collected on slides (Superfrost Plus; Fisher Scientific, Pittsburgh, PA). Cells were fixed with 4% formaldehyde (Sigma-Aldrich) for 10 min at room temperature followed by washing with 1% PBS. After the fixation, the cells were permeated with blocking buffer (0.5% BSA, 0.005% saponin, 0.02%  $\text{NaN}_3$ ) for 1 h at room temperature. The following primary antibodies were used: mouse anti-Lamp1 (Hybridoma Bank 1D4B), rat anti-Lamp1 (Santa Cruz 1D4B: sc19992), rabbit anti-LC3B (1:100, Novus bio NB100-2220), rabbit anti-Cone-Arrestin (1:1,000, EMD Millipore, AB15282), mouse anti-Ezrin to detect total Ezrin (1:100, Novex, 357300), rabbit anti-phospho-Ezrin (Th567) to detect phosphorylated form of Ezrin at threonine 567 (1:100, Sigma-Aldrich, PA5-37763), mouse anti-Rhodopsin (1:5000, Abcam, ab3267), rabbit serum anti-GFP (1:100, Life Technologies, A6455), rabbit anti-SQSTM1/p62 (1:1,000, Sigma-Aldrich, P0067), mouse anti-ZO-1 (1:100 Invitrogen #339100). All incubations were performed overnight at 4°C. After washing with 1% PBS, slides were incubated with the following secondary antibodies: Alexa 594 goat anti-rabbit/mouse/rat (1:1,000, Invitrogen A-11037 rabbit, A-11032 mouse) or Alexa 488 goat anti-rabbit/mouse/rat (1:1,000, Invitrogen A-11008 rabbit, A-11001 mouse) and DAPI (1:500, Vector Laboratories H-1200) for 1 h at room temperature; then, the slides were washed with 1% PBS and mounted with PBS/glycerol and imaged with a Zeiss LSM700 microscope. For detection of Lipofuscin autofluorescence in the RPE, confocal images were acquired by using excitation 543 nm and emission 570 nm as previously reported (Zhao *et al*, 2011). All samples were imaged, and images were identically processed. For phagosome counting, tissue sections were labeled with the Rhodopsin antibody. Confocal stacks of precisely 0.41- $\mu\text{m}$  thickness were acquired to yield maximal projections showing phagosomes in a constant tissue volume. ImageJ software was used for processing images, and the average number of phagosomes per 100  $\mu\text{m}$  of retina was calculated.

### Electron microscopy analysis

Mice retinæ were fixed using a mixture of 2% paraformaldehyde and 1% glutaraldehyde prepared in 0.2 M HEPES buffer (pH 7.4) for 24 h at 4°C. ARPE-19 cells were fixed with a mixture of 4% PFA and 0.05% GA for 10 min at room temperature, then washed with 4% PFA once to remove the residual GA, and fixed again with 4% PFA for 30 min at room temperature. Next, the cells were incubated with a blocking/permeabilizing mixture (0.5% BSA, 0.1% saponin, 50 mM  $\text{NH}_4\text{Cl}$ ) for 30 min and subsequently with the primary monoclonal antibody against LAMP1, diluted 1:500 in blocking/permeabilizing solution. The following day, the cells were washed and incubated with the secondary antibody, the anti-mouse Fab fragment coupled to 1.4 nm gold particles (diluted 1:50 in blocking/permeabilizing solution) for 2 h at room temperature. All specimens (retina and cells) were then post-fixed as described in Ref. (Polishchuk & Polishchuk, 2013). After dehydration, the specimens were embedded in epoxy resin and polymerized at 60°C for 72 h. Thin 60-nm sections were cut on a Leica EM UC7 microtome. EM images were acquired from thin sections using a FEI Tecnai-12 electron microscope equipped with a VELETTA CCD digital camera (FEI, Eindhoven, the Netherlands). Morphometric analysis on the size of lysosomes and the

distribution of gold particles (Lamp1-labeled) at the lysosomal structures was performed using iTEM software (Olympus SYS, Germany).

### Cone cell counts

Cone cell counts were performed as previously described (Barbato *et al*, 2017). Evaluation of the number of cones was performed by counting the cells positive for *cone-Arrestin* staining in standard areas at a comparable distance from the optic nerve. The number of cones/area was evaluated by manual counts with a Leica DM-6000 microscope, with the objective Leica  $\infty/0.17/D$ , HCX PL FLUOTAR, 40 $\times/0.75$  that has an area of 0.31  $\text{mm}^2$ .

**Expanded View** for this article is available online.

### Acknowledgements

We are grateful to Cathal Wilson, Antonella De Matteis, and Carmine Settembre for critical reading of the manuscript. We are grateful to Antonella Iuliano and Bioinformatic Core for statistical analysis at TIGEM. We are grateful to Carolina Iodice for technical support at TIGEM. Acknowledgement is made to the donors of the MDR, a program of the BrightFocus Foundation, for support of this research (Grant M2015317 to I.C.), to the Italian Telethon Foundation and the European Research Council [311682 “AlleleChoker” to E.M.S.]. This work was also supported by grants from the Italian Telethon Foundation (TGM16CB6 to A.B.); MIUR FIRB RBAP11Z3YA (A.B.); European Research Council Advanced Investigator no. 694282 (LYSOSOMICS to A.B.); U.S. National Institutes of Health (R01-NS078072 to A.B.); the Huffington Foundation (to A.B.); the Associazione Italiana per la Ricerca sul Cancro (Grants n.21052 and n. 22103 to A.B.).

### Author contributions

FN, DI, DF, CS, EP, GG, PT, EM, PS, and CDM performed the experiments and analyzed the data. IT and AA provided AAV 2/8-miR-211 mice. EMS, LJVG, SB, AB, and DLM contributed to the experimental design, implementation, and interpretation. EN and FGS contributed to the technical part of the work. IC conceived the experiments, analyzed the data, and wrote the manuscript. All authors read and approved the final manuscript.

### Conflict of interest

A.B. is Co-Founder of CASMA Therapeutics, Inc, Cambridge, MA 02139.

### References

- Abraham KJ, Chan JN, Salvi JS, Ho B, Hall A, Vidya E, Guo R, Killackey SA, Liu N, Lee JE *et al* (2016) Intersection of calorie restriction and magnesium in the suppression of genome-destabilizing RNA-DNA hybrids. *Nucleic Acids Res* 44: 8870–8884
- Alfano G, Conte I, Caramico T, Avellino R, Arno B, Pizzo MT, Tanimoto N, Beck SC, Huber G, Dolle P *et al* (2011) Vax2 regulates retinoic acid distribution and cone opsin expression in the vertebrate eye. *Development* 138: 261–271
- An J, Wang L, Guo Q, Li L, Xia F, Zhang Z (2012) Behavioral phenotypic properties of a natural occurring rat model of congenital stationary night blindness with *Cacna1f* mutation. *J Neurogenet* 26: 363–373
- Anderson DMG, Ablonczy Z, Koutalos Y, Hanneken AM, Spraggins JM, Calcutt MW, Crouch RK, Caprioli RM, Schey KL (2017) Bis(monoacylglycerol)

- phosphate lipids in the retinal pigment epithelium implicate lysosomal/endosomal dysfunction in a model of Stargardt disease and human retinas. *Sci Rep* 7: 17352
- Barbato S, Marrocco E, Intartaglia D, Pizzo M, Asteriti S, Naso F, Falanga D, Bhat RS, Meola N, Carissimo A et al (2017) MiR-211 is essential for adult cone photoreceptor maintenance and visual function. *Sci Rep* 7: 17004
- Barret C, Roy C, Montcourrier P, Mangeat P, Niggli V (2000) Mutagenesis of the phosphatidylinositol 4,5-bisphosphate (PIP(2)) binding site in the NH (2)-terminal domain of ezrin correlates with its altered cellular distribution. *J Cell Biol* 151: 1067–1080
- Bian K, Murad F (2014) sGC-cGMP signaling: target for anticancer therapy. *Adv Exp Med Biol* 814: 5–13
- Bonilha VL, Finnemann SC, Rodriguez-Boulan E (1999) Ezrin promotes morphogenesis of apical microvilli and basal infoldings in retinal pigment epithelium. *J Cell Biol* 147: 1533–1548
- Brambilla D, Fais S (2009) The Janus-faced role of ezrin in “linking” cells to either normal or metastatic phenotype. *Int J Cancer* 125: 2239–2245
- Bulut G, Hong SH, Chen K, Beauchamp EM, Rahim S, Kosturko GW, Glasgow E, Dakshnamurthy S, Lee HS, Daar I et al (2012) Small molecule inhibitors of ezrin inhibit the invasive phenotype of osteosarcoma cells. *Oncogene* 31: 269–281
- Celik H, Bulut G, Han J, Graham GT, Minas TZ, Conn EJ, Hong SH, Pauly GT, Hayran M, Li X et al (2016) Ezrin inhibition up-regulates stress response gene expression. *J Biol Chem* 291: 13257–13270
- Chou CH, Shrestha S, Yang CD, Chang NW, Lin YL, Liao KW, Huang WC, Sun TH, Tu SJ, Lee WH et al (2018) miRTarBase update 2018: a resource for experimentally validated microRNA-target interactions. *Nucleic Acids Res* 46: D296–D302
- Conley SM, Cai X, Makkia R, Wu Y, Sparrow JR, Naash MI (2012) Increased cone sensitivity to ABCA4 deficiency provides insight into macular vision loss in Stargardt's dystrophy. *Biochem Biophys Acta* 1822: 1169–1179
- Conte I, Merella S, Garcia-Manteiga JM, Migliore C, Lazarevic D, Carrella S, Marco-Ferreres R, Avellino R, Davidson NP, Emmett W et al (2014) The combination of transcriptomics and informatics identifies pathways targeted by miR-204 during neurogenesis and axon guidance. *Nucleic Acids Res* 42: 7793–7806
- Conte I, Hadfield KD, Barbato S, Carrella S, Pizzo M, Bhat RS, Carissimo A, Karali M, Porter LF, Urquhart J et al (2015) MiR-204 is responsible for inherited retinal dystrophy associated with ocular coloboma. *Proc Natl Acad Sci USA* 112: E3236–E3245
- Coscoy S, Waharte F, Gautreau A, Martin M, Louvard D, Mangeat P, Arpin M, Amblard F (2002) Molecular analysis of microscopic ezrin dynamics by two-photon FRAP. *Proc Natl Acad Sci USA* 99: 12813–12818
- Crepaldi T, Gautreau A, Comoglio PM, Louvard D, Arpin M (1997) Ezrin is an effector of hepatocyte growth factor-mediated migration and morphogenesis in epithelial cells. *J Cell Biol* 138: 423–434
- Cunnusamy K, Ufret-Vincenty R, Wang S (2012) Next-generation therapeutic solutions for age-related macular degeneration. *Pharm Pat Anal* 1: 193–206
- Dai X, Rao C, Li H, Chen Y, Fan L, Geng H, Li S, Qu J, Hou L (2015) Regulation of pigmentation by microRNAs: MITF-dependent microRNA-211 targets TGF-beta receptor 2. *Pigment Cell Melanoma Res* 28: 217–222
- Davidson AE, Millar ID, Burgess-Mullan R, Maher GJ, Urquhart JE, Brown PD, Black GC, Manson FD (2011) Functional characterization of bestrophin-1 missense mutations associated with autosomal recessive bestrophinopathy. *Invest Ophthalmol Vis Sci* 52: 3730–3736
- Erwig LP, McPhillips KA, Wynes MW, Ivetic A, Ridley AJ, Henson PM (2006) Differential regulation of phagosome maturation in macrophages and dendritic cells mediated by Rho GTPases and ezrin-radixin-moesin (ERM) proteins. *Proc Natl Acad Sci USA* 103: 12825–12830
- Federici C, Brambilla D, Lozupone F, Matarrese P, de Milito A, Lugini L, Iessi E, Cecchetti S, Marino M, Perdicchio M et al (2009) Pleiotropic function of ezrin in human metastatic melanomas. *Int J Cancer* 124: 2804–2812
- Fehon RG, McClatchey AI, Bretscher A (2010) Organizing the cell cortex: the role of ERM proteins. *Nat Rev Mol Cell Biol* 11: 276–287
- Ferrington DA, Sinha D, Kaarniranta K (2016) Defects in retinal pigment epithelial cell proteolysis and the pathology associated with age-related macular degeneration. *Prog Retin Eye Res* 51: 69–89
- Frost LS, Mitchell CH, Boesze-Battaglia K (2014) Autophagy in the eye: implications for ocular cell health. *Exp Eye Res* 124: 56–66
- Fuertes G, Martin De Llano JJ, Villarroya A, Rivett AJ, Knecht E (2003) Changes in the proteolytic activities of proteasomes and lysosomes in human fibroblasts produced by serum withdrawal, amino-acid deprivation and confluent conditions. *Biochem J* 375: 75–86
- Gargiulo S, Greco A, Gramanzini M, Esposito S, Affuso A, Brunetti A, Vesce G (2012) Mice anesthesia, analgesia, and care, Part II: anesthetic considerations in preclinical imaging studies. *ILAR J* 53: E70–E81
- Gary R, Bretscher A (1995) Ezrin self-association involves binding of an N-terminal domain to a normally masked C-terminal domain that includes the F-actin binding site. *Mol Biol Cell* 6: 1061–1075
- Gaynes BI, Torczynski E, Varro Z, Grostern R, Perlman J (2008) Retinal toxicity of chloroquine hydrochloride administered by intraperitoneal injection. *J Appl Toxicol* 28: 895–900
- Giatromanolaki A, Kalamida D, Sivridis E, Karagounis IV, Gatter KC, Harris AL, Koukourakis MI (2015) Increased expression of transcription factor EB (TFEB) is associated with autophagy, migratory phenotype and poor prognosis in non-small cell lung cancer. *Lung Cancer* 90: 98–105
- Guha S, Baltazar GC, Tu LA, Liu J, Lim JC, Lu W, Argall A, Boesze-Battaglia K, Laties AM, Mitchell CH (2012) Stimulation of the D5 dopamine receptor acidifies the lysosomal pH of retinal pigmented epithelial cells and decreases accumulation of autofluorescent photoreceptor debris. *J Neurochem* 122: 823–833
- Hall DP, Cost NG, Hegde S, Kellner E, Mikhaylova O, Stratton Y, Ehmer B, Abplanalp WA, Pandey R, Biesiada J et al (2014) TRPM3 and miR-204 establish a regulatory circuit that controls oncogenic autophagy in clear cell renal cell carcinoma. *Cancer Cell* 26: 738–753
- Hatano R, Fujii E, Segawa H, Mukaisho K, Matsubara M, Miyamoto K, Hattori T, Sugihara H, Asano S (2013) Ezrin, a membrane cytoskeletal cross-linker, is essential for the regulation of phosphate and calcium homeostasis. *Kidney Int* 83: 41–49
- He L, Hannon GJ (2004) MicroRNAs: small RNAs with a big role in gene regulation. *Nat Rev Genet* 5: 522–531
- Heiska L, Melikova M, Zhao F, Saotome I, McClatchey AI, Carpen O (2011) Ezrin is key regulator of Src-induced malignant phenotype in three-dimensional environment. *Oncogene* 30: 4953–4962
- Karali M, Peluso I, Gennarino VA, Bilio M, Verde R, Lago G, Dolle P, Banfi S (2010) miRNeve: a microRNA expression atlas of the mouse eye. *BMC Genom* 11: 715
- Keeling E, Lotery AJ, Tumbarello DA, Ratnayaka JA (2018) Impaired cargo clearance in the retinal pigment epithelium (RPE) underlies irreversible blinding diseases. *Cells* 7: E16
- Kim JY, Zhao H, Martinez J, Doggett TA, Kolesnikov AV, Tang PH, Ablonczy Z, Chan CC, Zhou Z, Green DR et al (2013) Noncanonical autophagy promotes the visual cycle. *Cell* 154: 365–376

- Kimura S, Noda T, Yoshimori T (2007) Dissection of the autophagosome maturation process by a novel reporter protein, tandem fluorescently-tagged LC3. *Autophagy* 3: 452–460
- Krishnan K, Bruce B, Hewitt S, Thomas D, Khanna C, Helman LJ (2006) Ezrin mediates growth and survival in Ewing's sarcoma through the AKT/mTOR, but not the MAPK, signaling pathway. *Clin Exp Metas* 23: 227–236
- Krol J, Busskamp V, Markiewicz I, Stadler MB, Ribi S, Richter J, Duebel J, Bicker S, Fehling HJ, Schubeler D et al (2010) Characterizing light-regulated retinal microRNAs reveals rapid turnover as a common property of neuronal microRNAs. *Cell* 141: 618–631
- Liang FQ, Anand V, Maguire AM, Bennett J (2001) Intraocular delivery of recombinant virus. *Methods Mol Med* 47: 125–139
- Lockwich T, Singh BB, Liu X, Ambudkar IS (2001) Stabilization of cortical actin induces internalization of transient receptor potential 3 (Trp3)-associated caveolar Ca<sup>2+</sup> signaling complex and loss of Ca<sup>2+</sup> influx without disruption of Trp3-inositol trisphosphate receptor association. *J Biol Chem* 276: 42401–42408
- Marion S, Hoffmann E, Holzer D, Le Clairche C, Martin M, Sachse M, Ganeva I, Mangeat P, Griffiths G (2011) Ezrin promotes actin assembly at the phagosome membrane and regulates phago-lysosomal fusion. *Traffic* 12: 421–437
- Matsui T, Maeda M, Doi Y, Yonemura S, Amano M, Kaibuchi K, Tsukita S, Tsukita S (1998) Rho-kinase phosphorylates COOH-terminal threonines of ezrin/radixin/moesin (ERM) proteins and regulates their head-to-tail association. *J Cell Biol* 140: 647–657
- Matsui T, Yonemura S, Tsukita S, Tsukita S (1999) Activation of ERM proteins *in vivo* by Rho involves phosphatidylinositol 4-phosphate 5-kinase and not ROCK kinases. *Curr Biol* 9: 1259–1262
- Medina DL, Di Paola S, Peluso I, Armani A, De Stefani D, Venditti R, Montefusco S, Scotto-Rosato A, Prezioso C, Forrester A et al (2015) Lysosomal calcium signalling regulates autophagy through calcineurin and TFEB. *Nat Cell Biol* 17: 288–299
- Mizushima N, Yamamoto A, Matsui M, Yoshimori T, Ohsumi Y (2004) *In vivo* analysis of autophagy in response to nutrient starvation using transgenic mice expressing a fluorescent autophagosome marker. *Mol Biol Cell* 15: 1101–1111
- Muniz-Feliciano L, Doggett TA, Zhou Z, Ferguson TA (2017) RUBCN/rubicon and EGFR regulate lysosomal degradative processes in the retinal pigment epithelium (RPE) of the eye. *Autophagy* 13: 2072–2085
- Nandrot EF, Chang Y, Finnemann SC (2008) Alpha5beta1 integrin receptors at the apical surface of the RPE: one receptor, two functions. *Adv Exp Med Biol* 613: 369–375
- Onyenwoke RU, Sexton JZ, Yan F, Diaz MC, Forsberg LJ, Major MB, Brenman JE (2015) The mucopolipidosis IV Ca<sup>2+</sup> channel TRPML1 (MCOLN1) is regulated by the TOR kinase. *Biochem J* 470: 331–342
- Ozeki N, Hase N, Hiyama T, Yamaguchi H, Kawai-Asano R, Nakata K, Mogi M (2017) MicroRNA-211 and autophagy-related gene 14 signaling regulate osteoblast-like cell differentiation of human induced pluripotent stem cells. *Exp Cell Res* 352: 63–74
- Ozturk DG, Kocak M, Akcay A, Kinoglu K, Kara E, Buyuk Y, Kazan H, Gozuacik D (2019) MITF-MIR211 axis is a novel autophagy amplifier system during cellular stress. *Autophagy* 15: 375–390
- Padanyi R, Xiong Y, Antalfy G, Lor K, Paszty K, Strehler EE, Enyedi A (2010) Apical scaffolding protein NHERF2 modulates the localization of alternatively spliced plasma membrane Ca<sup>2+</sup> pump 2B variants in polarized epithelial cells. *J Biol Chem* 285: 31704–31712
- Parameswaran N, Enyindah-Asonye G, Bagheri N, Shah NB, Gupta N (2013) Spatial coupling of JNK activation to the B cell antigen receptor by tyrosine-phosphorylated ezrin. *J Immunol* 190: 2017–2026
- Polishchuk EV, Polishchuk RS (2013) Analysis of Golgi complex function using correlative light-electron microscopy. *Methods Cell Biol* 118: 243–258
- Rizzolo LJ (2014) Barrier properties of cultured retinal pigment epithelium. *Exp Eye Res* 126: 16–26
- Sethna S, Chamakkala T, Gu X, Thompson TC, Cao G, Elliott MH, Finnemann SC (2016) Regulation of phagolysosomal digestion by caveolin-1 of the retinal pigment epithelium is essential for vision. *J Biol Chem* 291: 6494–6506
- Settembre C, Di Malta C, Polito VA, Garcia Arencibia M, Vetrini F, Erdin S, Erdin SU, Huynh T, Medina D, Colella P et al (2011) TFEB links autophagy to lysosomal biogenesis. *Science* 332: 1429–1433
- Settembre C, Medina DL (2015) TFEB and the CLEAR network. *Methods Cell Biol* 126: 45–62
- Sinha D, Valapala M, Shang P, Hose S, Grebe R, Luty GA, Zigler JS Jr, Kaarniranta K, Handa JT (2016) Lysosomes: regulators of autophagy in the retinal pigmented epithelium. *Exp Eye Res* 144: 46–53
- Strauss O (1995) The retinal pigment epithelium. In *Webvision: the organization of the retina and visual system*, Kolb H, Fernandez E, Nelson R (eds). Salt Lake City, UT. Retrieved from <http://www.ncbi.nlm.nih.gov/pubmed/2156333>
- Strauss O (2005) The retinal pigment epithelium in visual function. *Physiol Rev* 85: 845–881
- Tan LX, Toops KA, Lakkaraju A (2016) Protective responses to sublytic complement in the retinal pigment epithelium. *Proc Natl Acad Sci USA* 113: 8789–8794
- Turunen O, Wahlstrom T, Vaheri A (1994) Ezrin has a COOH-terminal actin-binding site that is conserved in the ezrin protein family. *J Cell Biol* 126: 1445–1453
- Vitiello M, Tuccoli A, D'Aurizio R, Sarti S, Giannecchini L, Lubrano S, Marranci A, Evangelista M, Peppicelli S, Ippolito C et al (2017) Context-dependent miR-204 and miR-211 affect the biological properties of amelanotic and melanotic melanoma cells. *Oncotarget* 8: 25395–25417
- Wan X, Mendoza A, Khanna C, Helman LJ (2005) Rapamycin inhibits ezrin-mediated metastatic behavior in a murine model of osteosarcoma. *Cancer Res* 65: 2406–2411
- Wang AL, Lukas TJ, Yuan M, Du N, Tso MO, Neufeld AH (2009) Autophagy and exosomes in the aged retinal pigment epithelium: possible relevance to drusen formation and age-related macular degeneration. *PLoS ONE* 4: e4160
- Wang FE, Zhang C, Maminishkis A, Dong L, Zhi C, Li R, Zhao J, Majerciak V, Gaur AB, Chen S et al (2010) MicroRNA-204/211 alters epithelial physiology. *FASEB J* 24: 1552–1571
- Xiao J, Zhu X, He B, Zhang Y, Kang B, Wang Z, Ni X (2011) MiR-204 regulates cardiomyocyte autophagy induced by ischemia-reperfusion through LC3-II. *J Biomed Sci* 18: 35
- Yao J, Jia L, Shelby SJ, Ganos AM, Feathers K, Thompson DA, Zacks DN (2014) Circadian and noncircadian modulation of autophagy in photoreceptors and retinal pigment epithelium. *Invest Ophthalmol Vis Sci* 55: 3237–3246
- Yao J, Jia L, Feathers K, Lin C, Khan NW, Klionsky DJ, Ferguson TA, Zacks DN (2016) Autophagy-mediated catabolism of visual transduction proteins prevents retinal degeneration. *Autophagy* 12: 2439–2450
- Young NP, Kamireddy A, Van Nostrand JL, Eichner LJ, Shokhirev MN, Dayn Y, Shaw RJ (2016) AMPK governs lineage specification through Tfeb-dependent regulation of lysosomes. *Genes Dev* 30: 535–552

- Zhang J, Bai Y, Huang L, Qi Y, Zhang Q, Li S, Wu Y, Li X (2015) Protective effect of autophagy on human retinal pigment epithelial cells against lipofuscin fluorophore A2E: implications for age-related macular degeneration. *Cell Death Dis* 6: e1972
- Zhang YQ, Fan YG, Dang YL, Liu YL, Liu H, Li LH (2017) Down-regulation of protein kinase C alpha/ezrin signals in light-induced phagocytic crisis of retinal pigment epithelium cells. *Int J Ophthalmol* 10: 1040–1045
- Zhang S, Ma H, Zhang D, Xie S, Wang W, Li Q, Lin Z, Wang Y (2018) LncRNA KCNQ1OT1 regulates proliferation and cisplatin resistance in tongue cancer via miR-211-5p mediated Ezrin/Fak/Src signaling. *Cell Death Dis* 9: 742
- Zhang C, Miyagishima KJ, Dong L, Rising A, Nimmagadda M, Liang G, Sharma R, Dejene R, Wang Y, Abu-Asab M et al (2019) Regulation of phagolysosomal activity by miR-204 critically influences retinal pigment epithelium/retinal structure and function. *Hum Mol Genet* 28: 3355–3368
- Zhao H, Shiue H, Palkon S, Wang Y, Cullinan P, Burkhardt JK, Musch MW, Chang EB, Turner JR (2004) Ezrin regulates NHE3 translocation and activation after Na<sup>+</sup>-glucose cotransport. *Proc Natl Acad Sci USA* 101: 9485–9490
- Zhao Z, Chen Y, Wang J, Sternberg P, Freeman ML, Grossniklaus HE, Cai J (2011) Age-related retinopathy in NRF2-deficient mice. *PLoS ONE* 6: e19456